[Prepared as a Contribution to *Discuss. Faraday Soc. No. 107*]

Interactions between Self-Assembled Monolayers and an Organophosphonate: A Detailed Study using Surface Acoustic Wave-Based Mass Analysis, Polarization Modulation-FTIR Spectroscopy, and Ellipsometry

Richard M. Crooks*,[1], Huey C. Yang, and Laurel J. McEllistrem

Department of Chemistry

Texas A&M University

College Station, TX 77843-3255

Ross C. Thomas and Antonio J. Ricco*,[2]

Microsensor R&D 1425

Sandia National Laboratories

Albuquerque, NM 87185-1425

[1]e-mail: crooks@chemvx.tamu.edu; fax: 409-845-1399; voice: 409-845-5629

[2]e-mail: ajricco@sandia.gov; fax: 505-844-1198; voice: 505-844-1405

*Authors to whom correspondence should be addressed.

Submitted: 24 June, 1997

Abstract

Self-assembled monolayers (SAMs) having surfaces terminated in the following functional groups: $-CH_3$, $-OH$, $-COOH$, and $-(COO^-)_2Cu^{2+}$ ($MUA-Cu^{2+}$) have been prepared and examined as potential chemically sensitive interfaces. Mass measurements made using surface acoustic wave (SAW) devices indicate that these surfaces display different degrees of selectivity and sensitivity to a range of analytes. The response of the $MUA-Cu^{2+}$ SAM to the nerve-agent simulant diisopropyl methylphosphonate (DIMP) is particularly intriguing. Exposure of this surface to 50%-of-saturation DIMP yields a surface concentration equivalent to about 20 DIMP monolayers. Such a high surface concentration in equilibrium with a much lower-than-saturation vapor pressure has not previously been observed. Newly developed analytical tools have made it possible to measure the infrared spectrum of the chemically receptive surface during analyte dosing. Coupled with *in-situ* SAW/ellipsometry measurements, which permit simultaneous measurement of mass and thickness with nanogram and Angstrom resolution, respectively, it has

DISCLAIMER

been possible to develop a model for the surface chemistry leading to the unusual behavior of this system. The results indicate that DIMP interacts strongly with surface-confined Cu^{2+} *via* the phosphoryl oxygen to yield a DIMP/Cu^{2+} adduct that nucleates growth of semi-ordered crystallites having substantially lower vapor pressure than the liquid.

Introduction

We recently demonstrated that composite self-assembled monolayers (SAMs), coupled with surface acoustic wave (SAW) device transducers, are effective chemical sensors for detection of vapor-phase organophosphonates (Figure 1).[1] In this Discussion we extend our investigation of chemistry at vapor/solid interfaces by examining interactions between SAMs having different terminal groups and vapor-phase diisopropyl methylphosphonate (DIMP, a nerve-agent simulant), with a view toward developing a better understanding of the molecular interactions between the SAMs and DIMP. The SAMs discussed here were prepared from 11-mercaptoundecanol (MUD), 11-mercaptoundecanoic acid (MUA), and MUA SAMs complexed with different with metal ions (MUA-M^{n+}). The results indicate that DIMP/SAM interactions arise from hydrogen bonds for the MUD and MUA SAMs and coordinative bonds for MUA-M^{n+} SAMs.

Figure 1

Dialkyl alkanephosphonates (methyl, ethyl, and isopropyl) have been extensively studied as model compounds for chemical warfare agents and pesticides.[2]

Many of these studies have focused on interactions between the phosphonates and metals,[3] metal oxides,[4] and metal salts.[5] The results of these studies suggest that the phosphoryl oxygen of the phosphonate is most responsible for this interaction. For example, DIMP reacts with many metal ions to form a complex that can be written as $M(DIMP)_nX_m$, where M is the metal and X is the counter ion.[5] Binding of organophosphonates by metal-free substrates has not attracted much attention because the resulting intermolecular interactions are relatively weak. For chemical sensor applications, however, such weak interactions can be advantageous since the likelihood of reversible analyte/substrate interactions is enhanced. Accordingly, we have chosen to examine SAMs with terminal groups capable of undergoing hydrogen-bonding interactions with DIMP, and compare these to MUA SAMs terminated with different metal ions.

In previous work, we showed that the magnitude of DIMP adsorption onto a SAM depends on at least four factors: the SAM endgroup, the time allotted for the SAM to assemble, the grain size of the Au onto which it assembles, and of course the concentration of DIMP in

the vapor phase.[1] The principal findings of these studies are as follows. First, a MUA-Cu^{2+} SAM is far more sensitive than a simple methyl-terminated SAM under any conditions studied, which suggests the presence of a specific interaction between MUA-Cu^{2+} and DIMP. Second, the amount of DIMP adsorbed on the MUA-Cu^{2+} SAM is a strong function of the time allotted for the SAM to assemble. For example, increasing the MUA formation time from 36 to 180 h yields roughly a five-fold increase in the adsorbed mass of DIMP. We ascribed this effect to time-dependent changes in SAM crystallinity. Third, for a particular set of dosing conditions, the mass of DIMP adsorbed onto the MUA-Cu^{2+} surface is a strong function of the underlying Au grain size, with the mass increasing as the grain size decreases. Finally, and most remarkably, the total mass of DIMP adsorbed onto a MUA-Cu^{2+} surface can be very high even at relatively modest vapor concentrations. For example, depending upon how the SAM is prepared, it can adsorb the equivalent of more than 20 monolayers of DIMP at half its saturation vapor pressure. We have postulated that this is a consequence of the extent and nature of the ordering of the SAM and its outer surface, and that these factors affect the

thermodynamics of adsorption. That is, the chemically sensitive SAM surface nucleates growth of a non-liquid-like DIMP phase having substantially lower vapor pressure than the bulk liquid. The principal purpose of the present Discussion is to gain a better understand of this unusual phenomenon.

Evidence for specific interactions between metal ions and phosphorus compounds comes from substantial frequency shifts of the P=O band in bulk solid-state materials.[6] We have found that frequency shifts of this band in the monolayer (and sometimes multilayer) complexes described here are more extreme than those in bulk phases, suggesting even stronger interactions. Both *in-situ* IR spectroscopy and SAW-based gravimetry confirm this suspicion.

To better understand the monolayer/DIMP chemistry, most data presented in this paper were obtained *in situ*. Specifically, we make use of polarization modulation-FTIR (PM-FTIR) spectroscopy, which provides real-time spectroscopic information about adsorbates even in the presence of large excesses of the corresponding vapor, and SAW/ellipsometry measurements, which permit

simultaneous measurement of the mass and thickness of adsorbates. The latter is particularly effective for discriminating between real and artifactual SAW-device responses arising from gross changes in the visco-elastic nature of thin films that can be induced by strongly interacting adsorbates. An excellent discussion of this effect is provided in the Discussion by Ricco *et al.* in this volume.[7]

Experimental Section

Chemicals. All chemicals were of reagent-grade quality or better, unless noted otherwise, and used without additional purification: diisopropyl methylphosphonate, DIMP (98%, Alfa); absolute ethanol (Midwest Grain Products); $AgNO_3$ (Alfa); $La(NO_3)_3 \cdot 6H_2O$ (Fisher Scientific); $CuCl_2 \cdot 2H_2O$ (EM Science). The following materials were purchased from the Aldrich Chemical Co.: $CH_3(CH_2)_{11}SH$ (98%, dodecanethiol, DDT); $CH_3(CH_2)_{10}COOH$ (98%, lauric acid); $Cu(ClO_4)_2 \cdot 6H_2O$; $Ni(ClO_4)_2 \cdot 6H_2O$; $Zn(NO_3)_2 \cdot 6H_2O$; $Fe(ClO_4)_3 \cdot 6H_2O$; $ZrOCl_2 \cdot xH_2O$. $HO(CH_2)_{11}SH$ (11-mercaptoundecanol, MUD) was synthesized from the analogous bromide. $COOH(CH_2)_{10}SH$ (11-mercaptoundecanoic acid, MUA) was synthesized according to a literature procedure.[8] Water was purified (resistivity > 18 MΩ-

cm) using a Milli-Q reagent water system (Millipore). Gaseous N_2 was obtained from liquid N_2 boil-off.

In-situ polarization modulation FTIR (PM-FTIR) spectroscopy. Au surfaces for PM-FTIR experiments were prepared by electron-beam evaporation of 10 nm of Ti or Cr followed by 200 nm of Au onto polished Si (100) wafers. The wafers were diced (3.3 cm x 0.95 cm), cleaned for 1 min in a low-energy Ar plasma cleaner (Harrick Scientific Model PDC-32G, Ossining, NY), immediately immersed in a 1 mM ethanolic thiol solution for 48 ± 5 h (unless otherwise noted), removed, rinsed with ethanol and water, and then dried in flowing N_2.[1,9] The metal-ion derivatized MUA SAMs were prepared identically, except they were subsequently soaked in a 5 mM ethanolic solution of the desired metal ion for 15 min, rinsed with ethanol, and then dried under flowing N_2.[1]

PM-FTIR measurements were made using a modified Mattson Research Series 1 infrared spectrometer (ATI Inc., Madison, WI). The infrared beam is passed through a ZnSe polarizer and a ZnSe photoelastic modulator (Hinds, model PEM90II/ZS37), reflected off the sample

surface at an incidence angle of 80°, passed through a focusing lens, and finally directed into a liquid N_2-cooled MCT detector. The photoelastic modulator is used to modulate the incident beam between *s*- (perpendicular) and *p*- (parallel) polarization with respect to surface normal. The real-time sampling electronics (Mattson) ratios the surface-insensitive *s*-polarized signal to the surface-sensitive *p*-polarized signal. This method obviates the need for a background spectrum.[10]

A custom-built vapor-phase flow cell was employed for all PM-FTIR measurements; it has been described in detail previously.[11] Two NaCl windows on the ends of the flow cell permit external reflection spectra to be recorded in a manner similar to normal *ex-situ* FTIR-ERS measurements. The partial pressure of the vapor-phase DIMP and the flow rate of the gas stream are determined by two mass-flow controllers: one controls a DIMP-saturated N_2 vapor and the other a pure N_2 gas stream, which is used to reduce the concentration of the saturated DIMP vapor. The vapor pressure of DIMP, measured using the Knudsen effusion method, was found to be 0.7 ± 0.3 mmHg at 25°C.[1a] The total flow rate

was set at 0.5 l/min for all experiments; therefore, a 10%-of-saturation DIMP concentration was obtained by mixing 0.05 l/min of the saturated DIMP stream with 0.45 l/min of N_2. The temperature for all PM-FTIR experiments was 23.5±1 °C.

PM-FTIR spectra of SAMs were obtained prior to dosing and subtracted from spectra obtained during dosing. Displayed spectra consist of 20 co-added cycles and each cycle consisted of 100 sum and 200 difference scans; total acquisition time was about 47 min per spectrum. Unless otherwise noted, the substrates were exposed to 10%-of-saturation DIMP vapor for 1 min prior to the first 47-min data acquisition period at this concentration. For most families of spectra, a spectrum was obtained while purging with pure N_2 between 48-78 min, and then, after dosing for 1 min with 50%-of-saturation DIMP, a spectrum was obtained between 79 - 126 min during dosing. The resolution of all spectra was 2 cm^{-1}.

IR transmission spectroscopy. IR transmission spectra were obtained at 2 cm^{-1} resolution using a Mattson Research Series 1 spectrometer equipped with a DTGS

detector. Vapor-phase DIMP spectra (20% of saturation), were obtained using a 10-cm gas cell (International Crystal Labs, Garfield, NJ) equipped with NaCl windows, which were O-ring sealed on each end. The cell was purged with pure N_2 for 30 min prior to introducing the analyte. Single-beam spectra of N_2 were used for the reference. Liquid-phase DIMP spectra were obtained by coating two NaCl salt plates with DIMP and pressing them together; this was referenced against a spectrum of the salt plates alone. Both vapor- and liquid-phase spectra consist of 32 scans. The solid-phase DIMP spectrum was obtained by freezing the salt plates containing liquid-phase DIMP in liquid N_2 and then measuring the spectrum immediately upon removal. This spectrum is the sum of 4 scans and took about 11 s to complete. All transmission spectra were obtained at an ambient temperature of 23.5±1 °C.

SAW and SAW/ellipsometry measurements. SAW devices (97 MHz) on ST-quartz with Ti-primed Au transducers were designed at Sandia National Laboratories (SNL) and custom fabricated at either SNL or by Lance Goddard Associates (Foster City, CA). In the active surface region between the transducers, 200 nm of Au was coated

over a Ti adhesion layer. If the SAW velocity is perturbed only by mass-loading variations, then the change in frequency, Δf, is related to the change in adsorbed mass per area, $\Delta(m/A)$, by eq 1

$$\Delta f/f_o = -\kappa c_m f_o \Delta(m/A) \qquad (1)$$

where c_m is the mass sensitivity (1.33 cm^2/g-MHz for ST-quartz), f_o is the unperturbed oscillator frequency (97 MHz), and κ is the fraction of the center-to-center distance between the transducers covered by the Au film; in the present case its value is 0.7. For the devices used here, a 1 ppm (97 Hz) decrease in frequency corresponds to 11 ng/cm^2. Assuming that adsorbed DIMP is spherical, has the density of the liquid (0.9849 g/cm^3), and that SAW-device frequency changes arise only from mass increases, an hexagonal close packed DIMP monolayer has a mass of 49 ng/cm^2 (equivalent to 4.5 ppm).

SAW data were obtained using a custom-built gas dosing system and electronics similar to those previously described.[9,11,12] A custom-built flow cell designed specifically for *in-situ* SAW/ellipsometry measurements

was used to obtain mass and thickness data simultaneously.[7] The cell was equipped with a pyrex glass window on each end to admit laser light at an angle of 70° relative to the surface normal. Other than this modification, the cell configuration was very similar to the flow cell described previously for mass-only measurements.[12] SAW-only and SAW/ellipsometry experiments were performed at 21.6±0.1 °C and 23.5±1 °C, respectively.

Ellipsometric measurements were made using a Gaertner Scientific model L2W26D.488 ellipsometer. Data were obtained using a He-Ne (632 nm) laser. Since all experiments were performed *in situ*, thicknesses were measured relative to the SAM surface. The refractive index was assumed to be 1.46 in all cases and data were recorded every minute. All other experimental conditions, including the Au-cleaning and SAM-preparation protocols, were identical to those described for the PM-FTIR experiments.

Results and Discussion

DIMP multilayer formation on a Cu^{2+}-terminated MUA SAM. Figure 2a shows frequency shift as a function of

vapor-phase concentration for six different organic analytes, as well as water, interacting with a SAW device coated with a MUA-Cu^{2+} SAM. The organomercaptan SAM was allowed to form for 180 h in this case. The data in Figure 2a indicate that multilayers form (based on molar volumes of the bulk liquids) at 50%-of-saturation vapor pressure (p/p_{sat} = 0.5) for all the analytes examined except *i*-octane. The number of multilayers that adsorb gives a qualitative indication of the "range" of the monolayer/analyte interaction. It is thus interesting to note that the frequency shift for DIMP at p/p_{sat} = 0.5 is consistent with the adsorption of approximately 22 layers of DIMP. This value is significantly larger than acetone, which has the next-highest equivalent mass coverage. DIMP is clearly the most amenable of the species examined to multilayer formation.

Figure 2

The methyl-terminated surface. In contrast to the results for the MUA-Cu^{2+} surface, Figure 2b shows SAW results (adsorption isotherms) for the same group of analytes interacting with a methyl-terminated SAM. In

this case, the SAM was allowed to form for 84 h. As illustrated in Figure 2b, there is no clear preference for the organophosphonate using this chemically insensitive interface. The same scales are used in both parts of Figure 2 to directly compare the response of the two monolayer films. Non-specific interactions between the analyte and the monolayer film (i.e., van der Waals forces) as well as specific interactions between adsorbing analyte molecules account for the relative differences in adsorbed mass.

Transmission IR spectroscopy of DIMP. To account for multilayer DIMP adsorption on some of the SAM surfaces at substantially lower-than-saturation vapor pressures, we propose that the SAM induces formation of a low-vapor-pressure surface phase of DIMP. Accordingly, it is necessary to fully understand the three bulk phases of DIMP prior to interpreting the surface spectra. Figure 3 shows spectra of the vapor, liquid, and solid phases of DIMP and Table 1 provides the peak assignments. The same general pattern of peaks is observed for all three phases. Three prominent stretching bands corresponding to the C-H modes of the isopropyl and P-bound methyl groups appear between 2850

and 3000 cm^{-1}. A number of bending modes arising from the same methyl groups are apparent: two sets of unresolved doublets between 1450-1475 cm^{-1} and 1370-1390 cm^{-1}, a singlet at 1310-1320 cm^{-1}, a triplet between 1100-1200 cm^{-1}, and another unresolved doublet in the 900-1050 cm^{-1} range.[13,14] The environmentally sensitive phosphoryl (P=O) stretching mode appears between 1200-1300 cm^{-1}, and the phosphate ester band is apparent as a very strong unresolved doublet between 980-1020 cm^{-1}.[13-16]

Figure 3

Table 1

A few observations are apparent when comparing the spectra for the three phases. First, the important P=O stretching mode (shaded in the figure) is at its lowest energy (1237 cm^{-1}) in the solid phase (vapor, 1266 cm^{-1}; liquid, 1245 cm^{-1}). Second, there are some substantial differences in relative peak intensities between the three phases. To facilitate comparison of the peak heights, the spectra in Figure 3 are plotted so the that the P=O band in all three phases is of constant height. Accordingly, the intensity of the 995

cm^{-1} vapor-phase PO-C band is about three times that of the liquid and solid. Similarly, the ratio of the intensity of the C-H stretching modes in $PC-H_3$ and $CC-H_3$ is highest in the vapor phase and lowest in the solid phase. These differences can be used to identify the phase behavior of DIMP when it is adsorbed at the vapor-solid interface.

Interactions between vapor-phase DIMP and surface-confined 11-mercaptoundecanol (MUD). Parts a, c, and d of Figure 4 show difference spectra for the MUD SAM during dosing with 10%-, 50%-, and 75%-of-saturation DIMP, respectively, and the spectrum obtained after dosing with 10%-of-saturation DIMP and then purging with pure N_2 for 30 min (part b of Figure 4). Peak assignments are given in Table 2. Recall that PM-FTIR spectra only reveal molecules near the Au surface, and because the spectrum of the MUD SAM (recorded in flowing N_2) has been subtracted from the data displayed in Figure 4, only bands corresponding to SAM-adsorbed DIMP, or SAM modes changed as a result of DIMP adsorption, will be apparent. Data obtained from unreactive methyl-terminated SAMs presented later confirm this assertion.

Figure 4

Table 2

Dosing with 10%-of-saturation DIMP results in a strong P=O stretching band at 1230 cm^{-1}, which is at significantly lower energy than the same mode in vapor- (1266 cm^{-1}) or liquid-phase (1245 cm^{-1}) DIMP and most closely correlates with the P=O band in the solid (doublet: 1237, 1220 cm^{-1}). The downward energy shift of this band in surface-adsorbed DIMP is likely a consequence of hydrogen bonding between the phosphoryl oxygen of DIMP and the hydroxyl group of the MUD SAM.[13d,17] When the DIMP vapor concentration is increased to 50% of saturation (part c of Figure 4) the phosphoryl band becomes an unresolved doublet with peaks at 1249 and 1230 cm^{-1}, which correspond to the pure-liquid and hydrogen-bonded phases, respectively. That is, at the higher DIMP concentration there are two distinct types of DIMP on the surface: the first monolayer, which is hydrogen bonded to the SAM, and subsequent layers that are not strongly hydrogen bonded. At even higher DIMP concentrations this trend continues: at 75% of saturation (part d of Figure 4)

the higher energy band at 1249 cm^{-1} dominates and the band corresponding to the hydrogen-bonded phase at 1230 cm^{-1} is present only as a weak shoulder indicating the presence of several non-hydrogen-bonded layers of DIMP.

It worth noting that the intensity of the hydrogen-bonded P=O band does not increase at DIMP concentrations higher than 10% of saturation, suggesting that the surface hydroxyl groups are completely covered by a monolayer of DIMP at this concentration. In other words, the hydrogen bond between the SAM hydroxyl groups and the DIMP P=O bond define the extent of adsorption at low concentrations, but other (presumably weaker) interactions not strongly correlated to the P=O band are responsible for adsorption of subsequent layers. Interestingly, even the non-hydrogen-bonded surface phase of DIMP is different than that of the pure liquid: there are clear differences in the band intensities in part d of Figure 4 and the liquid-phase spectrum in Figure 3. For example, the peak intensity at 1020 cm^{-1} is stronger than that of 997 cm^{-1} for the surface phase, but this trend is reversed for the liquid PO-C mode. In the high-energy part of the surface spectrum the C-H

stretching mode at 2980 cm^{-1} attributable to PC-H_3 is strong, while the hydrocarbon modes arising from CC-H_3 are nearly absent; the latter bands are more prominent in the liquid-phase spectrum. These differences may be a consequence of the surface IR selection rule, which states that dipoles having components normal to the metal surface are enhanced relative to those dominated by parallel dipoles, and suggest some degree of ordering in the DIMP surface phase.[18]

The final important point relevant to Figure 4 is that the interaction between the vapor-phase DIMP and the MUD SAM is fully reversible. This effect is illustrated in part b of Figure 4, which was obtained by dosing MUD SAM with 10%-of-saturation DIMP and then purging with pure N_2 for 30 min: the spectral features attributable to DIMP disappear after N_2 purging.

Interactions between vapor-phase DIMP and surface-confined 11-mercaptoundecanoic acid (MUA). We further investigated the effect of hydrogen bonding on adsorption by examining the interactions between an acid-terminated MUA SAM and DIMP. Because the liquid-

phase acidity of acids is higher than the corresponding alcohols, we hypothesized that the carboxylic acid surface would interact more strongly with the phosphoryl oxygen of DIMP than the hydroxyl surface. Figure 5 shows IR difference spectra of MUA during dosing with 5%-, 10%-, 30%-, 50%-, and 75%-of-saturation DIMP. The peak assignments are given in Table 2. As for the MUD SAM, peak intensities increase with increasing dosing concentration. A strong interaction between DIMP and the MUA surface is suggested by several of the peaks in Figure 5. The peak centered at 1208 cm^{-1} results from a strongly hydrogen-bonded phosphoryl group; it is shifted 37 cm^{-1} toward lower energy relative to liquid-phase DIMP, and the shift is about twice that observed for the MUD SAM-DIMP system. This finding strongly supports our contention that the first monolayer of DIMP interacts with the MUD and MUA SAMs *via* hydrogen bonding, and that the interaction is stronger in the MUA SAM. In contrast to the MUD system, DIMP does not saturate the MUA surface until higher dosing concentrations: about 30% of saturation for the MUA SAM (compared to 10% for MUD) judging from the growth of 1208 cm^{-1} band. This may be a consequence of the strong lateral hydrogen bonding

between acid groups in the MUA SAM or it may reflect a higher packing density than was observed for the MUD SAM.[19]

Figure 5

The derivative-shaped peaks in the acid-carbonyl region of the spectra in Figure 5 provide additional clues as to the nature of the DIMP-MUA interaction chemistry. As the concentration of DIMP increases, the peak at 1731 cm^{-1} increases and the one at 1710 cm^{-1} decreases. This is a consequence of the way DIMP interacts with the MUA SAM. Prior to DIMP exposure, the surface-IR spectrum of a MUA SAM indicates the presence of a mixture of non-hydrogen-bonded and hydrogen-bonded acid groups having acid carbonyl bands at 1739 and 1718 cm^{-1}, respectively.[1a,19] The derivative-shaped peaks present in Figure 5 after dosing result from two simultaneous effects. First, the lateral hydrogen bonds originally present in the MUA SAM are disrupted by the presence of DIMP, and the peak originally present at 1710 cm^{-1} decreases accordingly.[17a,b] Simultaneously, the interaction between the DIMP P=O group and the MUA acid gives rise to a new, but weaker, hydrogen bond

interaction that is manifested by the growth of the new band at 1731 cm^{-1}. That is, as the concentration of DIMP in the flow cell increases, the surface concentration of laterally hydrogen-bond MUA decreases while the amount of DIMP hydrogen bonded to MUA increases.

Other changes observed in the spectra shown in Figure 5 are in accordance with those noted earlier for the MUD SAM-DIMP system; these include the relative intensities of the hydrocarbon stretching bands at high energy and the phosphate ester doublet centered around 1010 cm^{-1}. As for the MUD SAM, the presence of two distinct forms of DIMP on the MUA surface at high dosing concentrations is observed. At low DIMP concentration (part a of Figure 5) a single P=O stretch is apparent at 1208 cm^{-1}, but as the concentration increases (parts c, d, and f of Figure 5) a new P=O stretching band grows in at 1247 cm^{-1}. The band at 1208 cm^{-1} corresponds to the first layer of DIMP strongly hydrogen bonded to MUA, while at higher dosing concentrations multilayers of DIMP form that are too far from the SAM surface to interact with it as strongly and the peak at 1247 cm^{-1}, which is

characteristic of liquid-phase DIMP grows in, and at 75%-of-saturation DIMP dominates this spectral region. Thus, just as for the MUD SAM, we find a strongly hydrogen-bonded first layer of DIMP on the MUA SAM at low dosing concentrations and additional layers of non-hydrogen-bonded DIMP at higher dosing concentrations.

Although purging the MUA SAM with N_2 promptly removes DIMP previously adsorbed during low-concentration dosing, DIMP dosed onto the surface at higher concentrations (> 50% of saturation) is removed much more slowly. Part e of Figure 5 shows the IR difference spectrum obtained after dosing with 50%-of-saturated DIMP and then purging with N_2 for 30 min. Essentially all DIMP is removed from the surface. Even the disrupted MUA lateral hydrogen bonding returns to its original state as indicated by the absence of the derivative shape in part e of Figure 5.

We were able to confirm the peak assignments, particularly those related to hydrogen bonding between DIMP and MUA, using transmission FTIR. In this experiment a thin layer of solution-cast lauric acid was applied to a NaCl plate and then mixed with a drop

of pure DIMP. The IR spectrum of the solid-state lauric acid prior to addition of DIMP reveals the strong C=O stretch of the face-to-face carboxylic acid dimer centered at 1693 cm^{-1} (spectrum not shown).[17] Upon addition of neat liquid-phase DIMP, the acid dimer band at 1693 cm^{-1} is replaced by a new carbonyl band at 1725 cm^{-1} and the characteristic DIMP bands, including the phosphoryl band at its characteristic hydrogen-bonded frequency of 1206 cm^{-1}. Similar results obtained when a thin film of lauric acid confined to a NaCl plate was exposed to vapor-phase DIMP in an IR gas cell: the C=O stretch shifts to 1727 cm^{-1} and hydrogen-bonded P=O stretching mode is present at 1204 cm^{-1}. These two important control experiments unambiguously support the notion that DIMP adsorbs onto the chemically sensitive MUD and MUA surfaces *via* hydrogen-bonding interactions between the phosphoryl oxygen and surface hydroxyl or acid groups, respectively.

On the basis of our observations, we propose the reaction mechanism for the MUA SAM-DIMP system shown in Scheme 1. Prior to dosing, the MUA SAM surface consists of non-hydrogen-bonded and laterally hydrogen bonded acid groups. After dosing with > 30%-of-saturation

DIMP, a multilayer structure forms on the surface: some of the DIMP is strongly hydrogen bonded to the MUA while the rest is present in a more weakly bound configuration. Additionally, the lateral hydrogen bonds initially present between acid groups are lost. At lower dosing concentrations, a monolayer or submonolayer of DIMP forms on the MUA surface. Upon purging with N_2, all DIMP is removed from the surface and the acid groups recover their original hydrogen-bonded configuration.

Scheme 1

Interactions between vapor-phase DIMP and surface-confined dodecane thiol (DDT). To confirm the importance of the hydrogen-bonding interaction between DIMP and the hydroxyl- and acid-terminated SAMs, we prepared a DDT SAM and dosed it with DIMP exactly as described for the MUD and MUA SAMs. The DDT SAM is terminated in a low-energy, methyl surface and is not likely to interact strongly with a polar compound like DIMP. Figure 6 shows PM-FTIR difference spectra of a DDT SAM during dosing with 10%-, 50%-, and 75%-of-saturation DIMP. The peak assignments are listed in

Table 2. We observe an appreciable IR signal for DIMP on the DDT surface only at the highest dosing concentration, and the peak positions are characteristic of the condensed liquid phase. For example, only a single phosphoryl band is present at 1247 cm^{-1}. Of course this weakly physisorbed DIMP is easily removed upon purging with N_2: part c of Figure 6 is a spectrum obtained after dosing with 50% of DIMP and then purging with pure N_2 for 30 min. This important control experiment also confirms proper implementation of the PM-FTIR apparatus since there is no spectral evidence for vapor-phase DIMP in the flow-cell headspace in part a of Figure 6. Finally, these spectroscopic experiments are qualitatively confirmed by the SAW-based gravimetric analysis shown in part b of Figure 2.

Figure 6

Interactions between vapor-phase DIMP and surface-confined 11-mercaptoundecanoic acid (MUA) complexed with Cu^{2+}. We showed previously that metal-ion-terminated MUA SAMs are easily prepared.[1] Figure 7 shows PM-FTIR difference spectra of a Cu^{2+}-modified MUA

SAM (MUA-Cu^{2+}), prepared by dipping a MUA SAM into an ethanolic solution of $Cu(ClO_4)_2$ and rinsing with ethanol, during dosing with 10%- and 50%-of-saturation DIMP (parts a and c, respectively) and after purging with N_2 for 30 min (parts b and d, respectively). Peaks assignments for this experiment, and others involving DIMP dosing of metal-ion-complexed surfaces, are provided in Table 3.

Figure 7

Table 3

During dosing with 10%-of-saturation DIMP, several spectral features indicate strong interactions between vapor-phase DIMP and the composite film. First, the intense band present at 1079 cm^{-1} corresponds to the P=O stretching mode of metal-ion-complexed DIMP. It is known that the phosphoryl oxygen of many phosphorus-containing compounds coordinate with metal ions to yield adducts characterized by a dramatic shift to lower energy of this band.[5,20] Typically, the metal-ion-complexed P=O band lies between 1100 and 1215 cm^{-1} depending upon the phosphorus compound, metal ion, and counter ion.[5] For example, Guilbault and Das[5g] exposed

metal-chloride solids to vapor-phase DIMP and found a shift in the P=O band from 1266 cm^{-1} (vapor-phase) to 1167 cm^{-1} for $FeCl_3$, and to 1232 and 1212 cm^{-1} (doublet) for $HgCl_2$. Our data for many MUA-M^{n+} surfaces indicate a shift of between 1060-1090 cm^{-1} for the P=O band (Table 3). We attribute this larger shift to the substantial differences between the SAM surfaces discussed in this work and the ionic solids described earlier. For example, the counter ions (perchlorate, nitrate, or chloride) used in previous studies will not influence the P=O band position in our experiments since the metal is initially coordinated to MUA; x-ray photoelectron (XPS) and IR spectroscopy results indicate the absence of anions other than the carboxylate.[21] We further confirmed the absence of anions other than carboxylate on the SAM surface by preparing metal-ion-complexed substrates from both $Cu(ClO_4)_2$ and $CuCl_2$ and noting no difference in the position of the P=O band.

Bands corresponding to the conversion of the carboxylate salt (negative bands at 1592 and 1437 cm^{-1}), arising from the strong Cu^{2+}-$(COO^-)_2$ interaction, to the acid form of MUA (positive acid-

carbonyl band at 1737 cm^{-1}) are also observed upon dosing with DIMP. Although the negative carboxylate bands are broad and somewhat indistinct in Figure 7, they are much sharper and intense for some of the other metal-ion-terminated SAMs (see Supporting Material). Finally, a variety of other bands directly attributable to the C-H and O-C modes of DIMP are present in the spectrum of the MUA-Cu^{2+} surface.

We interpret the four spectra shown in Figure 7 in terms of the model illustrated in Scheme 2. Prior to DIMP exposure (top frame of Scheme 2) MUA is complexed to Cu^{2+}, which bears coordinating water ligands. Upon exposure to DIMP (middle frame), we propose that the carboxylate surface becomes protonated, accounting for the observed spectral changes in the acid-group bands discussed earlier, as a consequence of the very strong interaction between DIMP and Cu^{2+}. That is, Cu^{2+} complexed to the carboxylate groups prior to dosing binds to DIMP during dosing, and the resulting $-COO^-$ groups are protonated by water originally ligated to Cu^{2+} or otherwise present on the high-energy MUA-Cu^{2+} surface. The result of this reaction gives rise to a Cu^{2+}/DIMP complex on the MUA surface, which is

presumably charge compensated by nearby hydroxyl ions formed by the same reaction that leads to MUA protonation. DIMP now interacts both through hydrogen bonding with the MUA surface (as discussed earlier for the metal-ion-free MUA surface, Figure 5) and by coordinative interactions with Cu^{2+}. These aspects of the model are supported, respectively, by the presence of the hydrogen-bonded P=O band centered at 1214 cm^{-1} (parts a and c of Figure 7, dashed line), and the greatly shifted P=O band at 1079 cm^{-1} arising from Cu^{2+}-complexed DIMP.

Scheme 2

The reaction between DIMP and the MUA-Cu^{2+} surface is partially irreversible. This is apparent because most of the key bands shown in part a of Figure 7 are still present after purging with N_2 (part b). Indeed, some of these bands actually increase after purging with N_2 for 30 min. The origin of this enhancement is not clear, but it is fully reversible and reproducible, suggesting that it might arise from a reversible orientational change of the P=O dipole or a change in the absorption coefficient of this band.[18]

One very important spectral change occurs in the after-N_2 purging spectrum that supports the model shown in Scheme 2. Upon exposure to N_2, the carbonyl band, present after dosing with 10%-of-saturation DIMP at 1737 cm^{-1}, splits into a doublet having peaks centered at 1737 and 1710 cm^{-1}. We attribute the doublet to the removal of DIMP bound to the MUA surface through the relatively weak hydrogen-bonding interaction. Thus, as shown in the bottom frame of Scheme 2 and signaled by the new 1710 cm^{-1} band, the now-protonated MUA SAM regains its intramonolayer lateral hydrogen bonds.

When the surface is dosed with a higher concentration of DIMP after N_2 purging (part c of Figure 7) several spectral observations consistent with Scheme 2 are observed. First, all of the peak intensities arising from DIMP increase substantially except the Cu^{2+}-associated P=O band (1079 cm^{-1}), which remains constant. This indicates that whatever surface concentration of Cu^{2+}-complexed DIMP is present on the surface after initial 10%-of-saturation exposure survives N_2 purging and cannot be increased by increasing the vapor-phase concentration of DIMP. In

other words, after the initial dosing, all Cu^{2+} sites remain coordinated to DIMP for the duration of the experiment. Second, note that the carbonyl band arising from laterally hydrogen bonded MUA acid groups disappears upon dosing with 50%-of-saturation DIMP. This is a consequence of the lateral MUA hydrogen bonds being replaced with DIMP/MUA hydrogen bonds as evidenced by the return of the corresponding peak at 1214 cm^{-1} in part c of Figure 7. Third, a new peak, not originally present at low dosing concentration, appears at 1246 cm^{-1}. This is the P=O band arising from uncomplexed DIMP, and its position is consistent with that found for the liquid phase (Table 1). One final observation is worth noting. There is a very weak band of approximately constant height present in all the spectra shown in Figure 7 at 2417 cm^{-1}. This peak might arise from a PO-H stretch,[22] which could result from the irreversible hydrolysis of DIMP.[5h] There is no trace of this peak on the unmetallated SAMs, but it is clearly visible on all of the metal-complexed SAMs (see Supporting Material). This is the only evidence we have observed for such a process, but it could represent a minor channel for the DIMP surface chemistry.

SAW/Ellipsometry data. It is well established that small changes in the viscoelastic properties of organic thin films can affect the frequency changes of SAW devices, and that such changes can be confused with mass changes.[7] In the present study we were quite concerned about the potential for perturbations in the mechanics of the MUA monolayer since it changes from metal-ion complexed to the laterally hydrogen-bonded acid form, and thereafter toggles between being hydrogen bonded to itself or DIMP. Therefore, we developed a flow cell suitable for simultaneous SAW and ellipsometric measurements that permits direct correlation of mass and thickness changes.

Figure 8 shows plots of simultaneously measured film thickness and SAW frequency shift as a function of time during exposure of a MUA-only SAM to DIMP/N_2 mixtures and N_2-only. Qualitatively, the figure shows that exposure of the SAW device to DIMP leads to a simultaneous increase in both thickness and mass (negative frequency changes correspond to mass increases). In region a, the SAW device was dosed with 10%-of-saturation DIMP, which yields a frequency shift

of 5 ppm, which is equivalent to 110% of a single DIMP monolayer. The measured thickness is 4 Å. The calculated diameter of a single DIMP molecule based on the liquid-phase DIMP density is 8.4 Å. Recognizing that the model used to fit the ellipsometric data assumes a layer of homogeneous thickness rather than an ensemble of spheres, which has a corrugated surface, the measured value of 4 Å correlates very well to single-monolayer adsorption.[23] Therefore, both the mass and thickness measurements are in accord and indicate approximately monolayer adsorption.

Figure 8

In region b there was a baseline shift in the SAW response, so we measured the frequency for dosing with 30%-of-saturation DIMP from the after-dosing baseline. This approach yields a doubling of the mass of adsorbed DIMP, which correlates well with the doubling in the measured ellipsometric thickness to 8 Å. Similar changes are observed at higher dosing concentrations (regions c and e). The spikes in the SAW data in region e, which are also apparent in the ellipsometry data, may reflect bulk condensation of DIMP on the acid

surface. When we repeated the measurement at 30%-of-saturation DIMP (region d) we obtained a mass increase about 30% higher than the prior measurement at this dosing concentration, which may be a consequence of the baseline shift observed during the first measurement at this concentration since the thicknesses are about the same in both cases. There is a slight drift in the thickness-measurement baseline that amounts to less than 1 Å/h, but we do not believe it significantly affects the measurements.

The main points to be derived from this experiment are that both the mass and thickness data are consistent with one another and the PM-FTIR data discussed earlier. For example, the results indicate an increase in the mass of adsorbed DIMP as the vapor-phase concentration increases and that sorption/desorption of DIMP from the MUA-only surface is fully reversible on the time-scale of these experiments. It is particularly satisfying that at a dosing concentration of 50% of saturation the SAW results indicate 4-5 monolayers of DIMP on the surface, while in the completely independent PM-FTIR experiment the non-hydrogen-bonded signature of DIMP appears at 1247 cm^{-1} (part d of

Figure 5) at this same DIMP concentration. This provides additional evidence for a hydrogen-bonding interaction between the first monolayer of DIMP and the MUA SAM, but at surface concentrations exceeding this level DIMP adsorbs to the surface through interactions spectroscopically indistinguishable from those of the liquid.

Figure 9 shows SAW/ellipsometry data analogous to that just discussed, but for the MUA-Cu^{2+} surface. During the initial 10%-of-saturation DIMP dosing cycle there is a mass change corresponding to 3 DIMP monolayers and a thickness change of 8 Å, which is reasonably consistent with the mass loading data. Both the SAW and ellipsometry results indicate about half the DIMP present at the end of the dosing cycle remains irreversibly bound to the MUA-Cu^{2+} surface after N_2 purging. This strongly suggests that, in contrast to the MUA-only surface, much of the first monolayer-equivalent of DIMP remains very strongly bound to the MUA-Cu^{2+} surface. This result is in excellent agreement with the PM-FTIR results, which lends further credence to the model presented in Scheme 2.

Figure 9

Dosing with 50%-of-saturation DIMP adds an additional 9 monolayers of DIMP to the irreversibly bound material already present. The additional increase in ellipsometric thickness of about 23 Å is in only rough agreement with the mass measurement. Errors resulting from our approximation that DIMP is a spherical molecule are likely to be exacerbated at high coverages, which may account for the discrepancy. The SAW/ellipsometry data correlate well with the PM-FTIR results (part c of Figure 7), which reveal the appearance of a liquid-phase-DIMP-correlated P=O peak at 1246 cm^{-1} at this dosing concentration. Upon N_2 purging both the SAW and ellipsometry data indicate a return to the pre-50%-of-saturation DIMP dosing level (but note the slight drift in the ellipsometry baseline). Partial removal of DIMP from the surface is also consistent with the PM-FTIR data (part d of Figure 7).

When the MUA-Cu^{2+} surface is again dosed with 10%-of-saturation DIMP a change in SAW frequency corresponding to about 2 DIMP monolayers is observed, but when purged

with N_2 it all desorbs excluding the portion that irreversibly adsorbed to the surface at the beginning of the experiment.

Summary and Conclusions

We have shown that the MUA-Cu^{2+} surface provides a selective and sensitive interface for binding the nerve-agent simulant DIMP. Remarkably, depending on how it is prepared, this surface can bind more than 20 monolayer-equivalents of DIMP when dosed with 50%-of-saturation DIMP.[1] We conclude that the MUA-Cu^{2+} surface enhances ordering of the DIMP layers and acts as a template for growth of a low-vapor-pressure phase that is distinct from the liquid. We can offer no other thermodynamically viable alternative explanation for the observations presented here. For example, it is not reasonable to postulate long-range forces acting between the outer DIMP layers and the SAM that extend over distances of more than 150 Å (the approximate equivalent of 20 monolayers of DIMP).

To better understand these results, we have used a combination of PM-FTIR spectroscopy, simultaneous, *in-*

situ SAW/ellipsometry measurements, and suitable control experiments to develop a model that accounts for the results. Scheme 2 illustrates the main points of this model. Upon initial dosing of the MUA-Cu^{2+} interface with DIMP, a monolayer or two of DIMP irreversibly complexes with Cu^{2+}, which results in protonation of the MUA SAM. The Cu^{2+}/DIMP complexes then act as nucleation points for growth of structured crystallites, which have a lower vapor pressure than liquid-phase DIMP. As the size of the crystallites increases the molecules within them become more disordered and accordingly there is a somewhat linear isotherm that connects the magnitude of surface adsorption to the vapor-phase DIMP concentration (Figure 2).

When N_2 is used to purge the Cu^{2+}/MUA/DIMP interface, DIMP is readily removed, except for that fraction irreversibly bound to Cu^{2+}. In contrast to this behavior, a MUA-only interface readily releases all DIMP from its surfaces when purged. Both the MUA-Cu^{2+} and MUA-only surfaces are capable of undergoing hydrogen-bonding interactions with DIMP, as is to a lesser extent the MUD interface. The unreactive methyl-

terminated DDT SAM adsorbs only a small fraction of the DIMP found on the other surfaces.

To the best of our knowledge, the MUA-Cu^{2+}/DIMP system is the first example of a tailored chemically sensitive surface to display such an unusual sorption isotherm. This important discovery should permit us to design better interfaces specifically constructed to demonstrate this function. This may help us achieve our goal of developing SAW-based chemical sensors that are simple to synthesize, highly sensitive, and that display a high degree of chemical class specificity.

Acknowledgment

Work at Texas A&M was supported by the National Science Foundation (CHE-9313441) and Sandia National Laboratories. We also acknowledge Mr. Daniel Dermody (Texas A&M University) for assistance with the SAW/ellipsometry experiments. Work at Sandia National Laboratories was supported by the United States Department of Energy under Contract DE-AC04-94AL85000. Sandia is a multiprogram laboratory operated by Sandia Corporation, a Lockheed Martin Company, for the United States Department of Energy.

Supporting Material Available

PM-FTIR spectra of MUA-M^{n+} (M=Ag^{+}, Cu^{2+} [from $CuCl_2$], Ni^{2+}, Zn^{2+}, Fe^{3+}, La^{3+}, Zr^{4+}) surface during DIMP dosing. Eight pages.

References

1. (a) L. J. Kepley, R. M. Crooks and A. J. Ricco, *Anal. Chem.*, 1992, **64**, 3191. (b) R. C. Thomas, H. C. Yang, C. R. DiRubio, A. J. Ricco and R. M. Crooks, *Langmuir*, 1996, **12**, 2239.

2. (a) M. A. Butler and A. J. Ricco, *Anal. Chem.*, 1992, **64**, 1851.(b) E. S. Kolesar, Jr. and R. M. Walser, *Anal. Chem.*, 1988, **60**, 1731. (c) E. S. Kolesar, Jr. and R. M. Walser, *Anal. Chem.*, 1988, **60**, 1737. (d) G. S. Groenewold and P. J. Todd, *Anal. Chem.*, 1985, **57**, 886. (e) E. S. Kolesar, Jr., C. P. Brothers, Jr., C. P. Howe, T. J. Jenkins, A. T. Moosey, J. E. Chin and J. M. Wiseman, *Thin Solid Films*, 1992, **220**, 30. (f) G. G. Guilbault, J. Affolter, Y. Tomita and E. S. Kolesar, Jr., *Anal. Chem.*, 1981, **53**, 2057.

3. (a) P. Koch, H. Rumpel, P. Sutter and C. D. Weis, *Phosphorus, Sulfur, and Silicon Relat. Elem.*, 1989, **44**, 75. (b) R. I. Hedge, C. M. Greenlief and J. M. White, *J. Phys. Chem.*, 1985, **89**, 2886.

4. (a) M. A. Henderson, T. Jin and J. M. White, *J. Phys. Chem.*, 1986, **90**, 4607. (b) M. K. Templeton and W.

H. Weinberg, *J. Am. Chem. Soc.*, 1985, **107**, 97. (c) M. K. Templeton and W. H. Weinberg, *J. Am. Chem. Soc.*, 1985, **107**, 774.

5. (a) N. M. Karayannis, C. Owens, L. L. Pytlewski and M. M. Labes, *J. Inorg. Nucl. Chem.*, 1970, **32**, 83. (b) G. G. Guilbault and E. P. Scheide, *J. Inorg. Nucl. Chem.*, 1970, **32**, 2959. (c) N. M. Karayannis, C. Owens, L. L. Pytlewski, L. L. Labes, *J. Inorg. Nucl. Chem.*, 1969, **31**, 2059. (d) N. M.Karayannis, L. L. Pytlewski, C. Owens, *J. Inorg. Nucl. Chem.*, 1980, **42**, 675. (e) N. M. Karayannis, C. M. Mikulski, M. J. Strocko, L. L. Pytlewski and M. M. Labes, *Inorganica Chim. Acta*, 1971, **5**, 357. (f) C. Owens, N. M. Karayannis, L. L. Pytleski, and M. M. Labes, *J. Phys. Chem.*, 1971, **75**, 637. (g) G. G. Guilbault and J. Das, *J. Phys. Chem.*, 1969, **73**, 2243. (h) T. Wagner-Jauregg, B. E. Hackley, Jr., T. A. Lies, T. A., O. O. Owens, O. O., R. J. Proper, *J. Am. Chem. Soc.*, 1955, **77**, 922.

6. F. A. Cotton, R. D. Barnes and R. D. Bannister, *J. Chem. Soc.*, 1960, 2199.

7. A. J. Ricco, A. W. Staton, R. M. Crooks, and T. Kim, *Discuss. Faraday Soc. No. 107*, submitted for publication.

8. C. D. Bain, E. B. Troughton, Y.-T. Tao, J. Evall, G. M. Whitesides and R. G Nuzzo, *J. Am. Chem. Soc.*, 1989, **111**, 321.

9. H. C. Yang, D. L. Dermody, C. Xu, A. J. Ricco and R. M Crooks, *Langmuir*, 1996, **12**, 726.

10. (a) M. J. Green, B. J. Barner and R. M. Corn, *Rev. Sci. Instrum.*, 1991, **62**, 1426. (b) B. J. Barner, M. J. Green, E. I. Saez and R. M. Corn, *Anal. Chem.*, 1991, **63**, 55.

11. (a) C. Xu, L. Sun, L. J. Kepley, R. M. Crooks and A. J. Ricco, *Anal. Chem.*, 1993, **65**, 2102. (b) R. M. Crooks, L. Sun, C. Xu, S. L. Hill and A. J. Ricco, *Spectroscopy*, 1993, **8**, 28, and references therein.

12. (a) A. J. Ricco, G. C. Frye and S. J. Martin, *Langmuir*, 1989, **5**, 273. (b) R. C. Hughes, A. J. Ricco,

M. A. Butler and S. J. Martin, *Science*, 1991, **254**, 74. (c) A. J. Ricco, *Interface*, 1994, **3**, 38.

13. R. A. McIvor, G. A. Grant and C. E. Hubley, *Can. J. Chem.*, 1956, **34**, 1611. (b) H. F. Hameka, A. H. Carrieri and J. O. Jensen, *Phosphorus, Sulfur, and Silicon Relat. Elem.*, 1992, **66**, 1. (c) J. W. Maarsen, M. C. Smit and J. Matze, *Recueil Trav. Chim. Pays-Bas*, 1957, **76**, 713. (d) A. E. T. Kuiper, J. J. G. M. van Bokhoven and J. Medema, *J. Catal.*, 1976, **43**, 154.

14. (a) L. C. Thomas and R. A. Chittenden, *Spectrochim. Acta*, 1965, **21**, 1905. (b) K. B. Mallion, F. G. Mann, B. P. Tong and V. P. Wystrash, *J. Chem. Soc.*, 1963, 148.

15. L. C. Thomas and R. A. Chittenden, *Spectrochim. Acta*, 1964, **20**, 467.

16. L. C. Thomas and R. A. Chittenden, *Spectrochim. Acta*, 1964, **20**, 489.

17. N. B. Culthup, L. H. Daly and S. E. Wiberley, *Introduction to Infrared and Raman Spectroscopy*; 3rd Ed., Academic Press: New York, 1990.

18. M. D. Porter, *Anal. Chem.*, 1988, **60**, 1143A.

19. (a) L. Sun, L. J. Kepley and R. M. Crooks, *Langmuir*, 1992, **8**, 2101. (b) L. Sun, R. M. Crooks and A. J. Ricco, *Langmuir*, 1993, **9**, 1775. (c) E. L. Smith, C. A. Alves, J. W. Anderegg and M. D. Porter, *Langmuir*, 1992, **8**, 2707. (d) R. V. Duevel and R. Corn, *Anal. Chem.*, 1992, **64**, 337.

20. D. M. L. Goodgame and F. A. Cotton, *J. Chem. Soc.*, 1961, 3735 and references therein.

21. G. Socrates, *Infrared Characteristic Group Frequencies*, John Wiley & Sons: Chichester, 1980.

22. D. Lin-Vien, N. B. Colthup, W. G. Fately, and J. G. Grasselli, *Infrared and Raman Characteristic Frequencies of Organic Molecules*, Academic: San Diego, 1991.

23. A. B. D. Cassi, *Discuss. Faraday Soc.*, 1948, **3**, 11.

Table 1. Peak assignments for vapor-, liquid-, and solid-state DIMP.

Assignment	Vapor/cm^{-1}	Liquid/cm^{-1}	Solid/cm^{-1}
$\nu_{PC-H_3}(a)$	2985	2979	2978
$\nu_{CC-H_3}(s)$	2945	2934	2932
ν_{PC-H_3} (?)	2886	2878	2877
$\delta_{CC-H_3}(a)$	1473, 1457	1468, 1455	1469, 1458
$\delta_{CC-H_3}(s)$	1387, 1377;sh	1386, 1375	1385, 1376
$\delta_{PC-H_3}(s)$	1314	1312	1315
$\nu_{P=O}$	1266	1245	1237, 1220;sh
δ_{CC-H_3}(rock)	1180,1142 1112	1178, 1142 1112	1180, 1145 1110
ν_{PO-C}	1018, 995	1011, 986	1010, 981
δ_{PC-H_3}(rock)	919, 901	917, 899	919, 903

sh, shoulder; a, asymmetric; s, symmetric

?, There is disagreement in the literature about this peak assignment. An alternative assignment is ν_{C-H}.

Assignments based on information in Reference 13-16.

Table 2. Peak assignments for DIMP (75% of saturation) during dosing of SAMs having different endgroups.

Assignment	MUD/cm^{-1}	MUA/cm^{-1}	DDT/cm^{-1}
$\nu_{PC-H_3}(a)$	2980	2979	n/o
$\nu_{CC-H_3}(s)$	2940	2934	n/o
$\delta_{CC-H_3}(a)$	1469, 1456	1467	n/o
$\delta_{CC-H_3}(s)$	1387, 1376	1387, 1376	1388, 1376
$\delta_{PC-H_3}(s)$	1312	1312	n/o
$\nu_{P=O}$	1249	1247	1247
$\nu_{P=O}$ (H-Bonded)	1231, sh	1208	n/o
δ_{CC-H_3}(rock)	1180, 1144 1111	1181, 1143 1112	1179, 1107
ν_{PO-C}	1020, 997	1021, 998	1016
δ_{PC-H_3}(rock)	n/o	919, 903	n/o

MUD,11-mercaptoundecanol; MUA, 11-mercaptoundecanoic acid; DDT, dodecanethiol; sh, shoulder; a, asymmetric; s, symmetric; n/o, not observed.

Assignments based on information in Reference 13-16.

Table 3. Peak assignments for prominent DIMP and metal-ion-terminated 11-mercaptoundecanoic acid (MUA) SAMs.during dosing with 50%-of-saturation DIMP. Peak energies are expressed in cm^{-1}.

Assignment	Ag^+	Cu^{2+}	Cu^{2+}	Ni^{2+}	Zn^{2+}	Fe^{3+}	La^{3+}	Zr^{4+}
Anion	NO_3^-	ClO_4^-	Cl^-	ClO_4^-	NO_3^-	ClO_4^-	NO_3^-	Cl^-
ν_{PC-H_3} (a)	2980	2980	2982	2980	2980	2980	2979	2981
ν_{CC-H_3} (s)	2940	2940	2942	2939	2939	2938	2938	2940
ν_{PC-H_3} (?)	2881	2876	2880	2877	n/o	2877	2879	n/o
$\nu_{C=O}$ (COOH)	1736	1737	1737	1740	1740	1741	1740	1740
ν_{COO^-} (a)	-1529	-1592	-1625	-1590	-1593	-1580	-1544	-1573
ν_{COO^-} (s)	-1406	-1437	-1421	-1436	1448 -1461	-1447	-1442	-1473 -1463
δ_{CC-H_3} (s)	1387 1376	1387 1376	1387 1376	1386 1376	1387 1376	1387 1376	1386 1376	1387 1376
δ_{PC-H_3} (s)	1313	1312	1313	1313	1312	1312	1313	1312
$\nu_{P=O}$	1246	1246	1247	1246	1246	1248	1246	1248
$\nu_{P=O}$ (H-Bonded)	1207	1214 1201	1207	1216	1212sh 1197	1214 1200	1214	1213 1201
δ_{CC-H_3} (rock)	1180 1143 1112	1179 1143 1112	1180 1144 1113	1180 1142 1109	1181sh 1142 1107	1180 1144 1125	1180 1142 1110	1179 1143 1114
$\nu_{M^{n+}P=O}$	1065	1079	1079	1076	1086	1089	1078	1083
ν_{PO-C}	1020 1000	1016 1000	1020 1003	1019 1003	1017 1003	1018 1002	1021 1002	1023 1002
δ_{PC-H_3}(rock)	920 901	917 900	917 904	918 901	917 901	917 904	918 900	918 899

?: There is disagreement in the literature about this peak assignment. An alternative assignment is ν_{C-H}.

n/o, not observed; "-", negative; a, asymmetric; s, symmetric; sh, shoulder.

Figure Captions

Figure 1. Schematic illustration of a composite self-assembled monolayer (SAM)-modified chemically sensitive SAW device. Selectivity for organophosphonate nerve-agent simulants can be modified by changing the SAM terminal groups or modifying the metal coordinated to MUA.

Figure 2. Adsorption isotherms for a SAW device coated with either a (a) MUA-Cu^{2+} or (b) CH_3-terminated SAM, exposed to six different organic analytes and water. Each isotherm was obtained over the course of 2 h. The same scales are used in both parts of the figure to directly compare the response of the two SAMs. In (a), the equivalent coverage for the DIMP analyte at 50%-of-saturation is about 22 layers. The SAM was allowed to form for 180 h.

Figure 3. Transmission FTIR spectra of bulk vapor-, liquid-, and solid-phase DIMP. The constant-height shaded region corresponds to the phosphoryl (P=O) band, which is normalized in the figure to facilitate comparison of the height of the other bands. Dotted

lines are intended to show shifts in the relative peak positions of the different phases for some bands discussed in the text.

Figure 4. PM-FTIR difference spectra of a 11-mercaptoundecanol (MUD) SAM during dosing with (a) 10%-, (c) 50%-, and (d) 75%-of-saturation DIMP, and (b) after dosing with 10%-of-saturation DIMP and then purging with N_2 for 30 min. The dashed line indicates the hydrogen-bonded phosphoryl band at 1231 cm^{-1}.

Figure 5. PM-FTIR difference spectra of a 11-mercaptoundecanoic acid (MUA) SAM during dosing with (a) 5%-, (b) 10%-, (c) 30%-, (d) 50%-, and (f) 75%-of-saturation DIMP, and (e) after dosing with 50%-of-saturation DIMP and then purging with N_2 for 30 min. The dashed line indicates the hydrogen-bonded phosphoryl band at 1208 cm^{-1} and enhanced non-hydrogen-bonded carboxylic acid band centered at 1731 cm^{-1}.

Figure 6. PM-FTIR spectra of a dodecanethiol (DDT) SAM during dosing with (a) 10%-, (b) 50%-, and (d) 75%-of-saturation DIMP, and (c) after dosing with 50%-of-

saturation dosing and then purging with N_2 for 30 min. The dashed line indicates the phosphoryl band at 1247 cm^{-1}.

Figure 7. PM-FTIR spectra of a MUA-Cu^{2+} SAM during dosing with (a) 10%- and (c) 50%-of-saturation, and then (b and d) purging with N_2 for 30 min. The dashed lines represent the hydrogen-bonded phosphoryl band at 1214 cm^{-1} and the non-hydrogen-bonded -COOH band at 1737 cm^{-1}. Note the change in scale for (c).

Figure 8. Simultaneous SAW/ellipsometry results for a MUA SAM during dosing with (a) 10%-, (b) 30%-, (c) 50%-, (d) 30%-, and (e) 75%-of-saturation DIMP. A pure-N_2 purge is introduced between DIMP dosing cycles.

Figure 9. Simultaneous SAW/ellipsometry results for a MUA-Cu^{2+} SAM during dosing with (a) 10%-, (b) 50%-, and (c) 10%-of-saturation DIMP. A pure N_2 purge is introduced between DIMP dosing cycles.

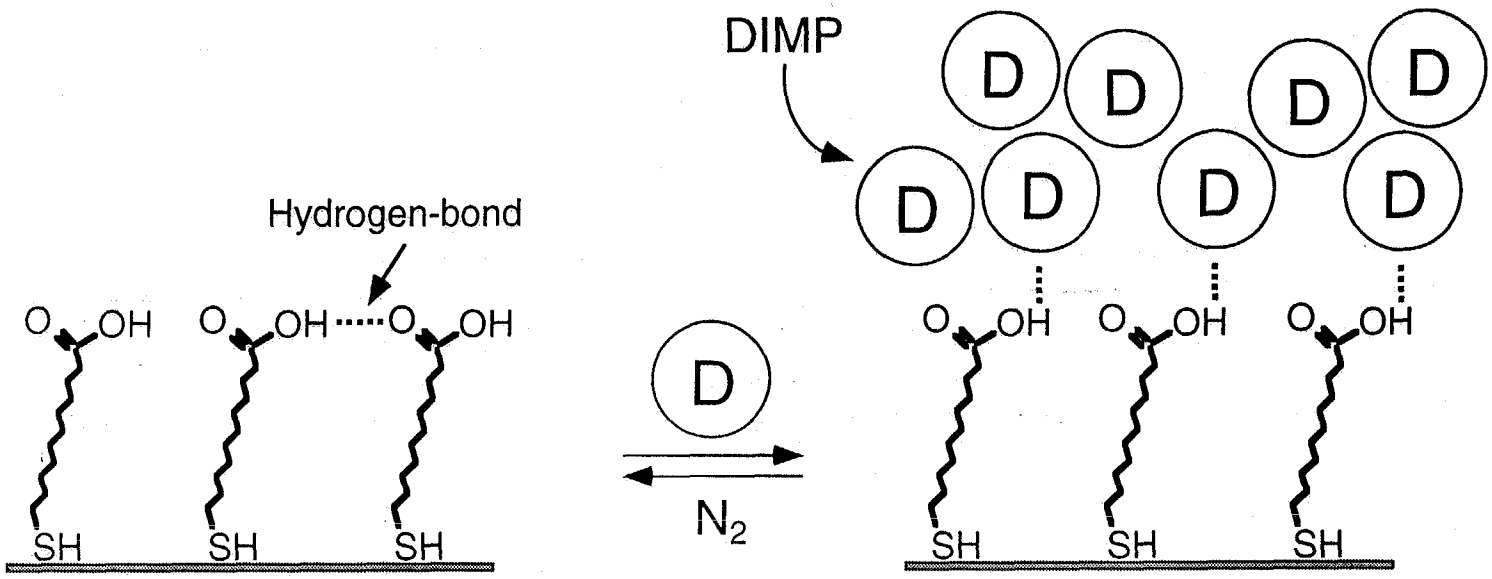

Scheme 1/Crooks et al.

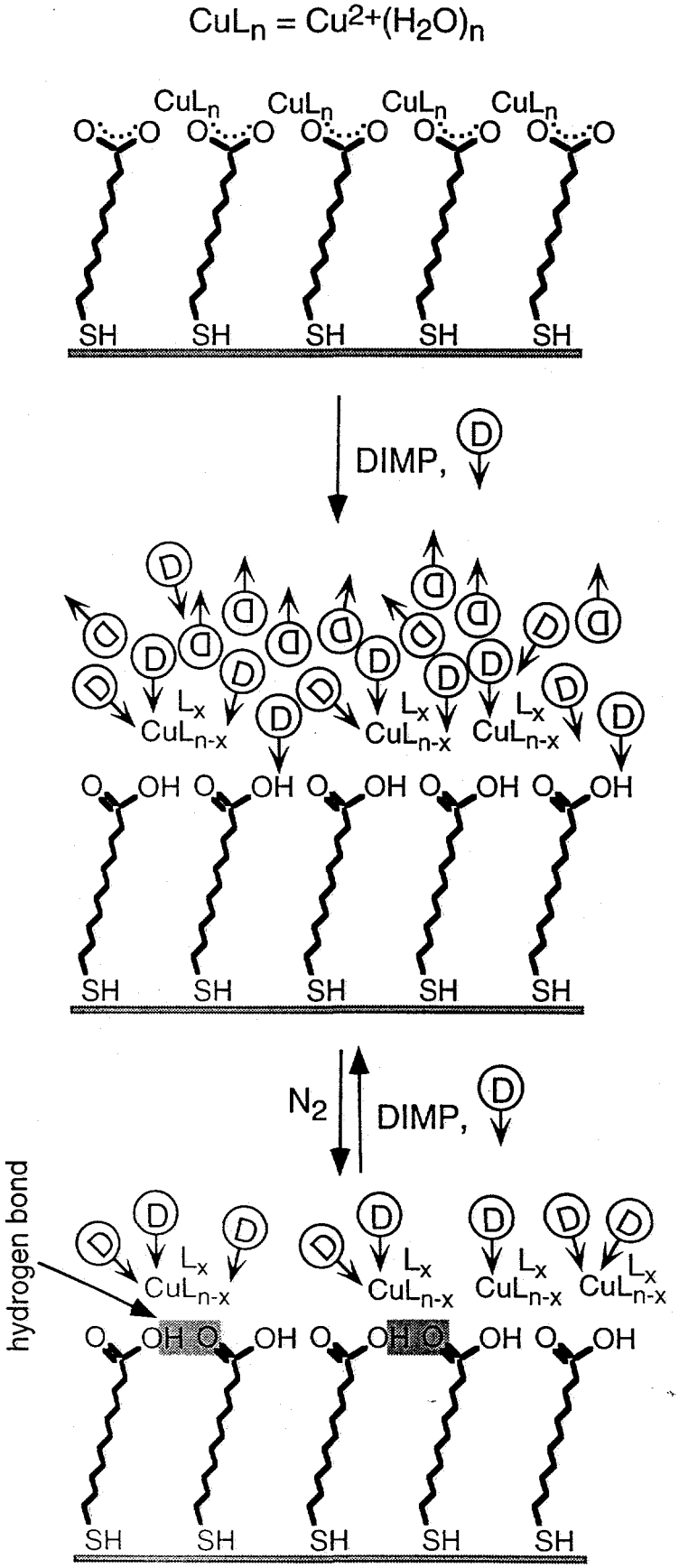

Scheme 2/Crooks et al.

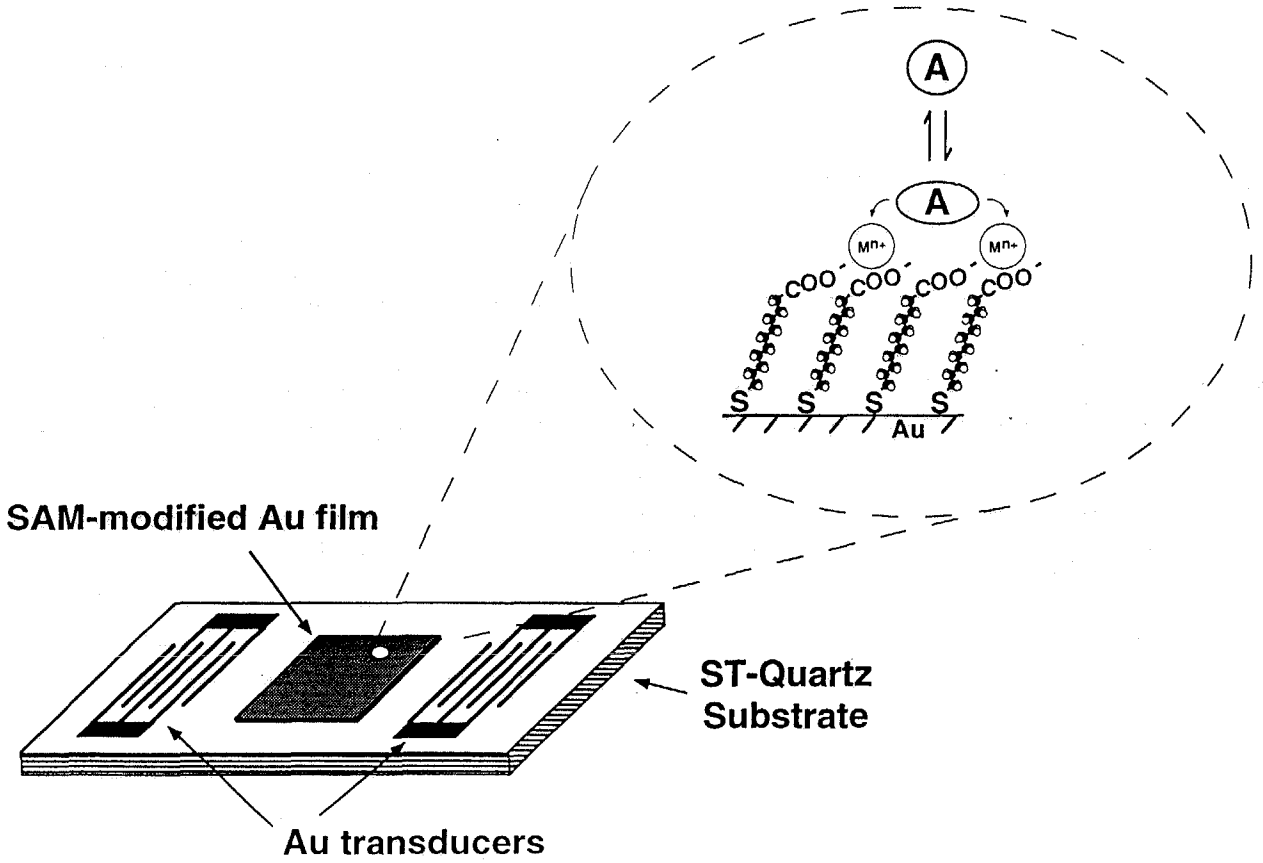

Figure 1/Crooks et al.

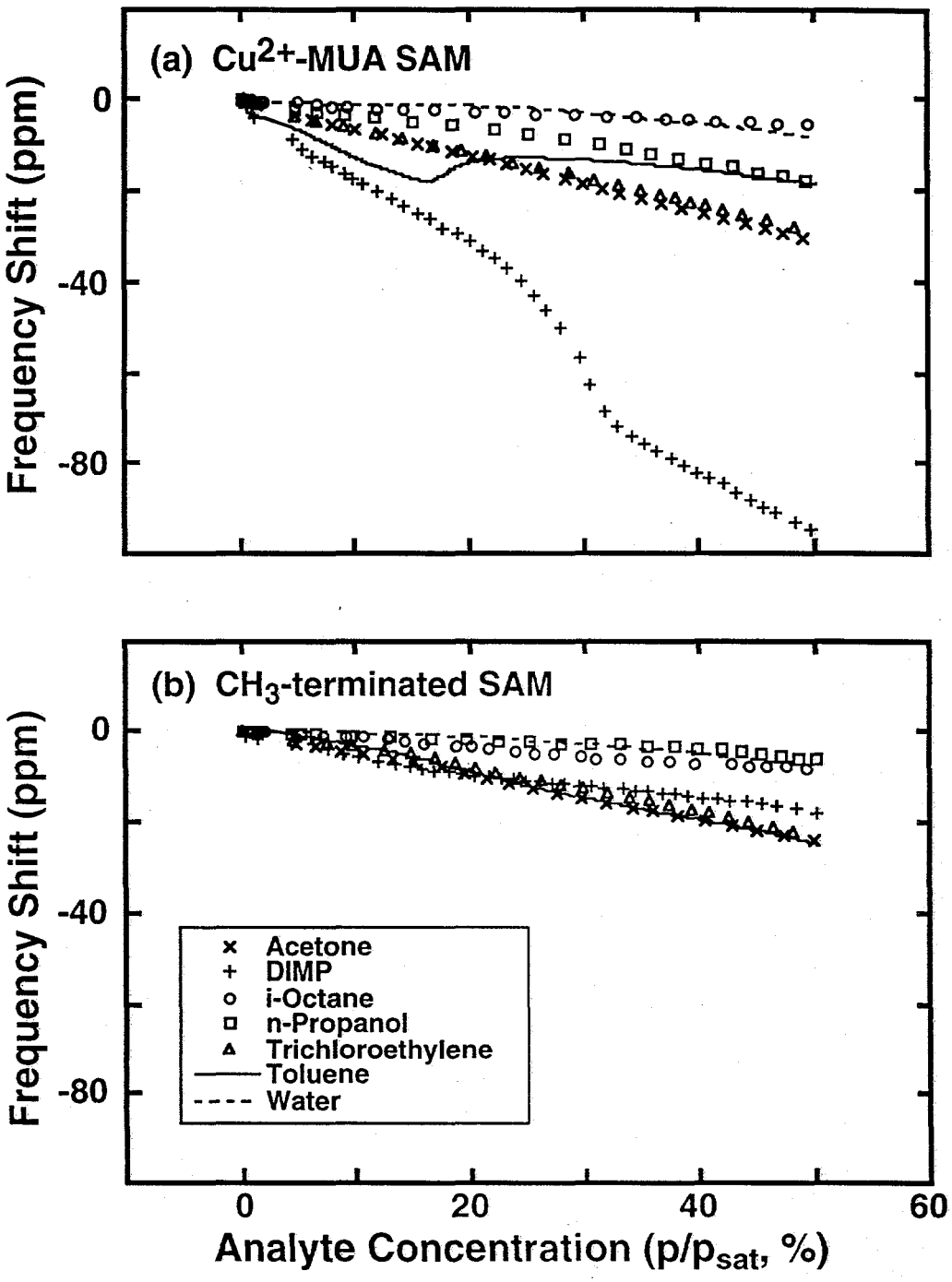

Figure 2/Crooks et al.

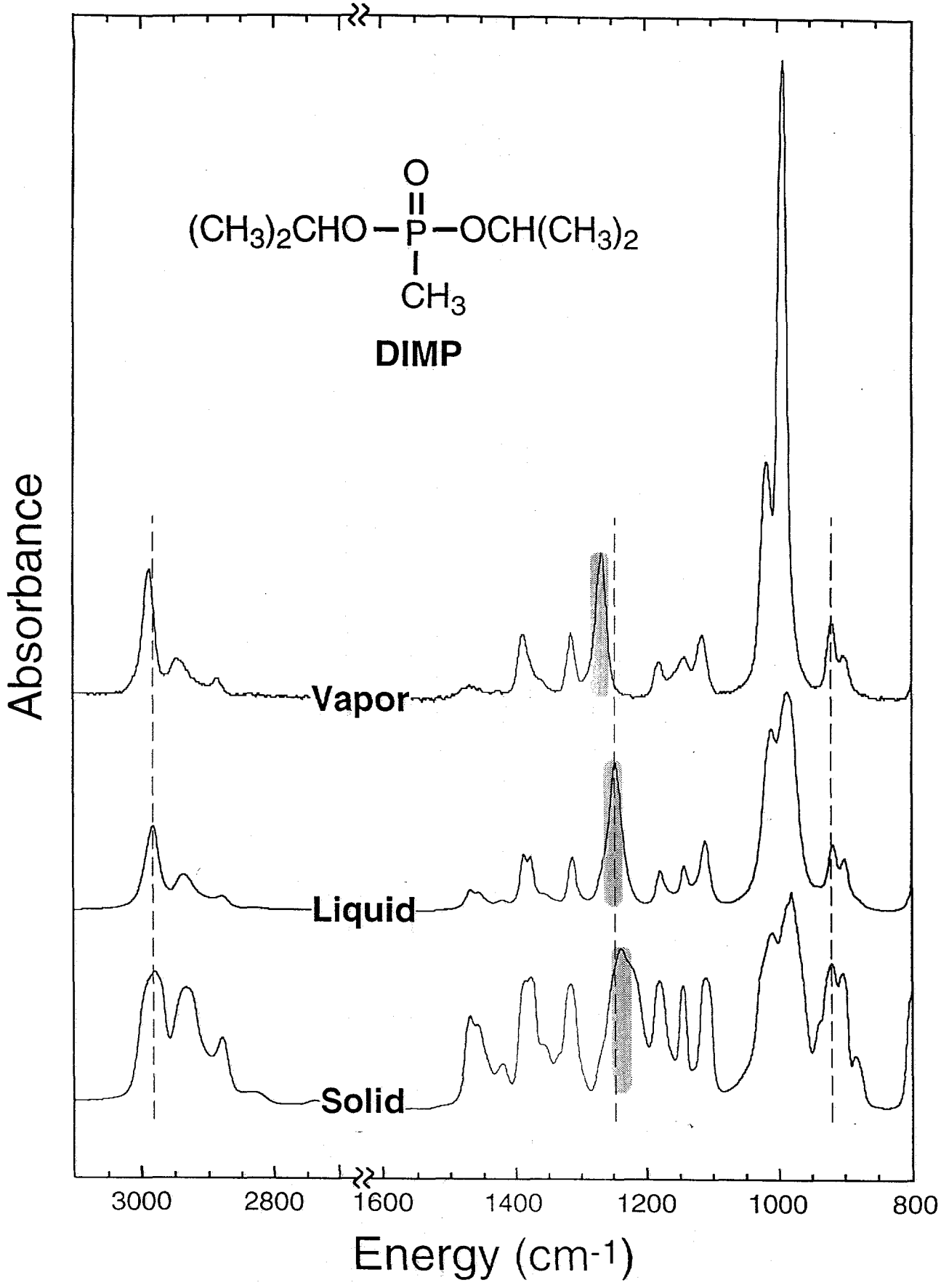

Figure 3/Crooks et al.

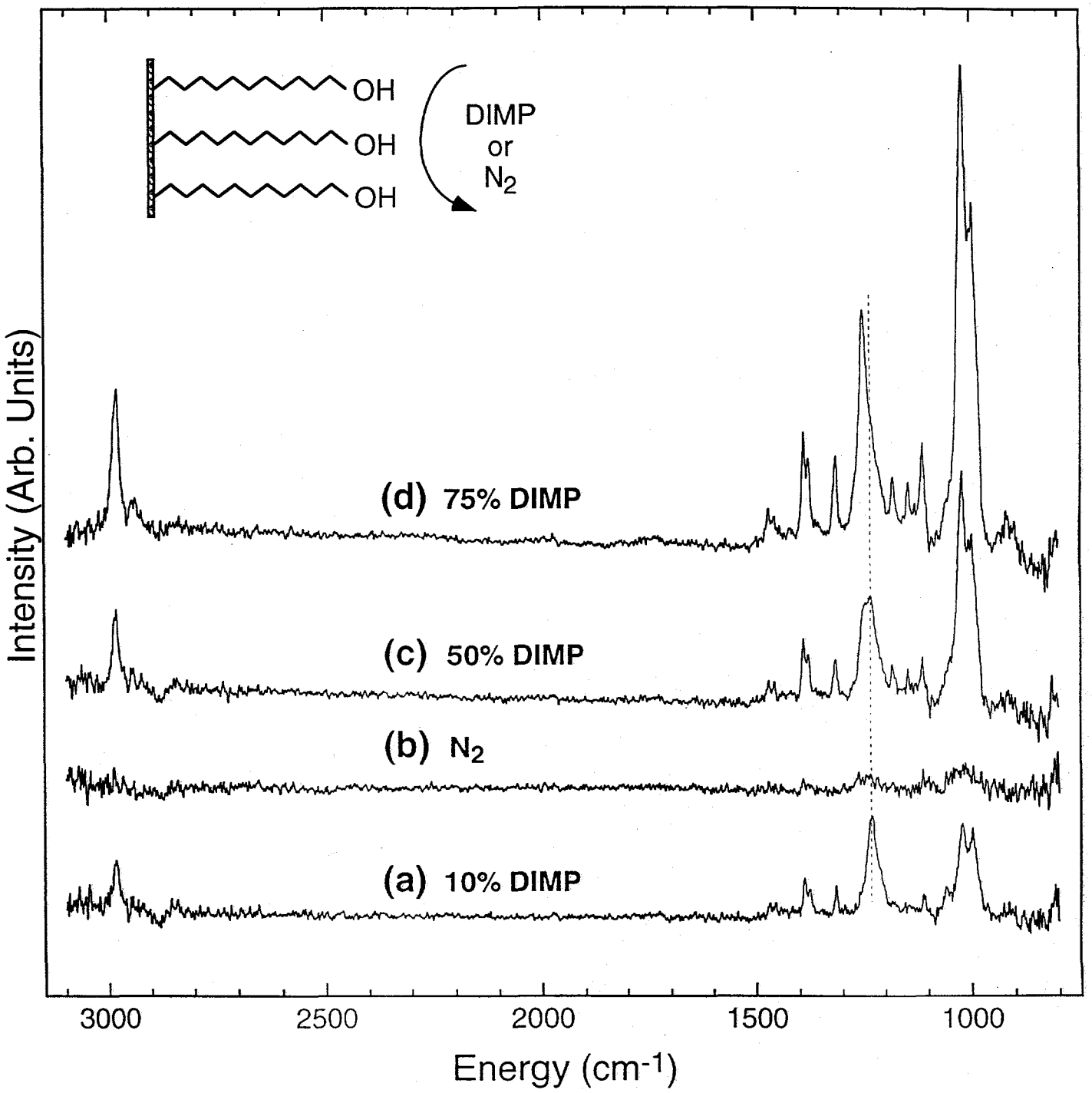

Figure 4/Crooks et al.

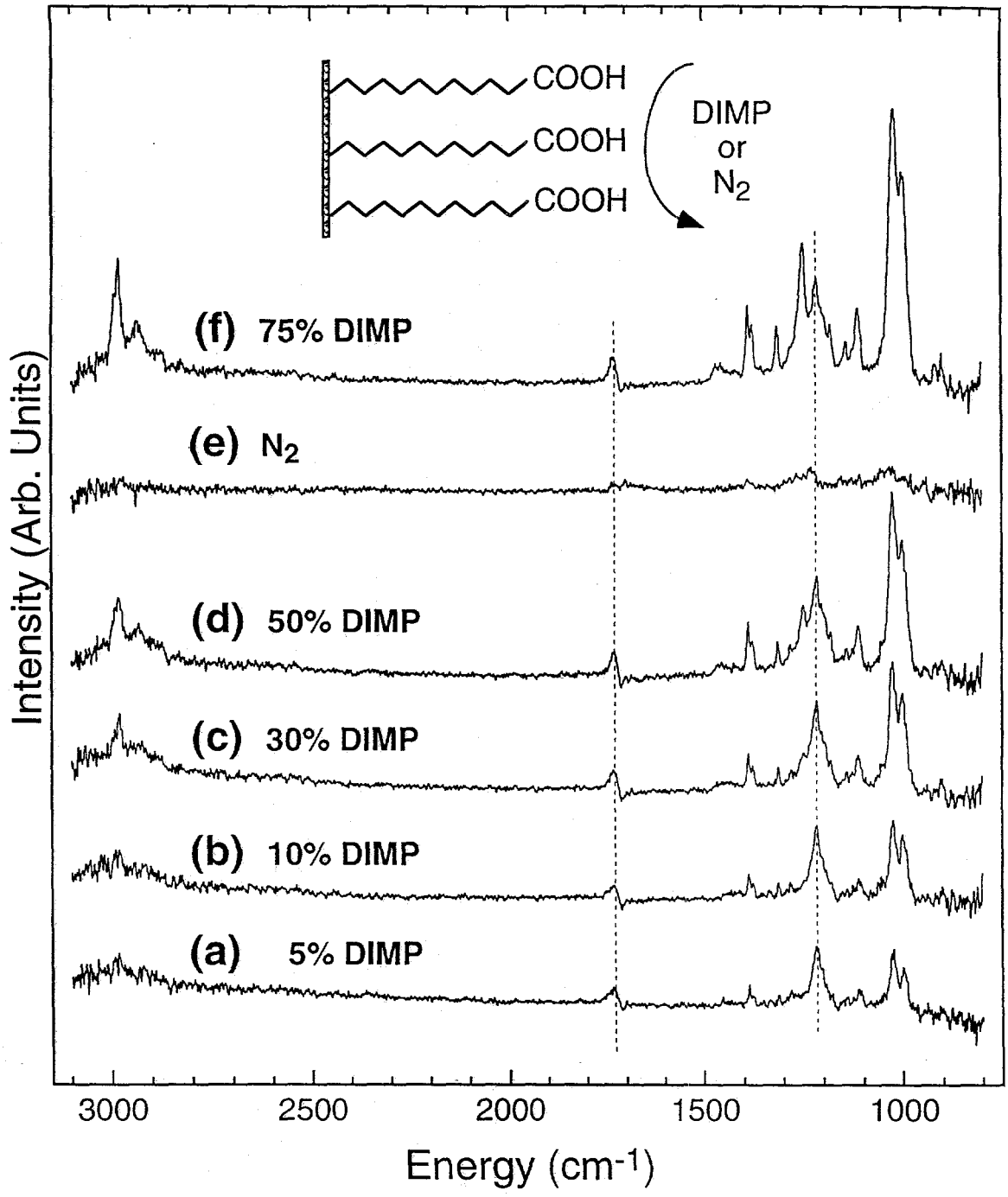

Figure 5/Crooks et al.

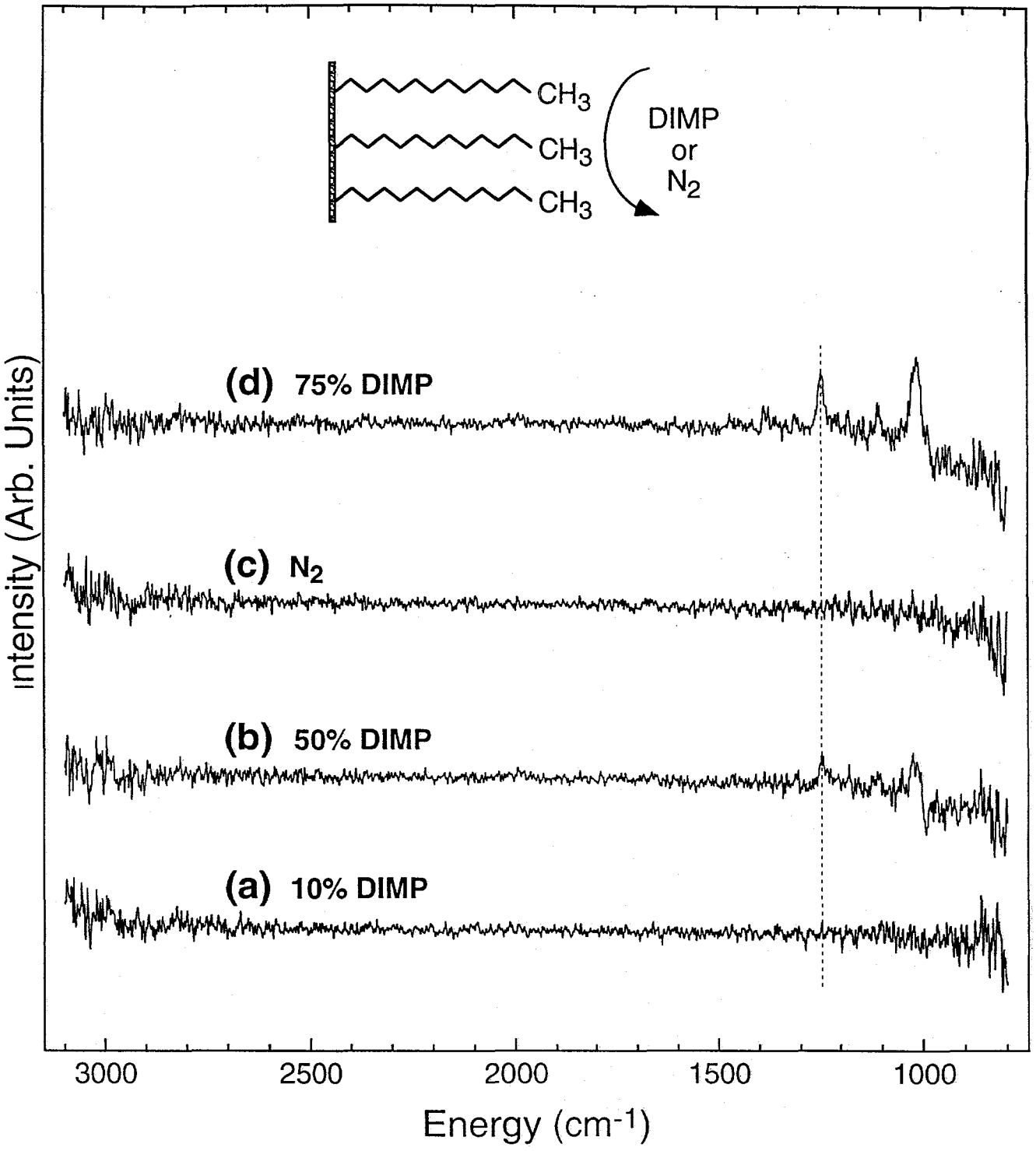

Figure 6/Crooks et a

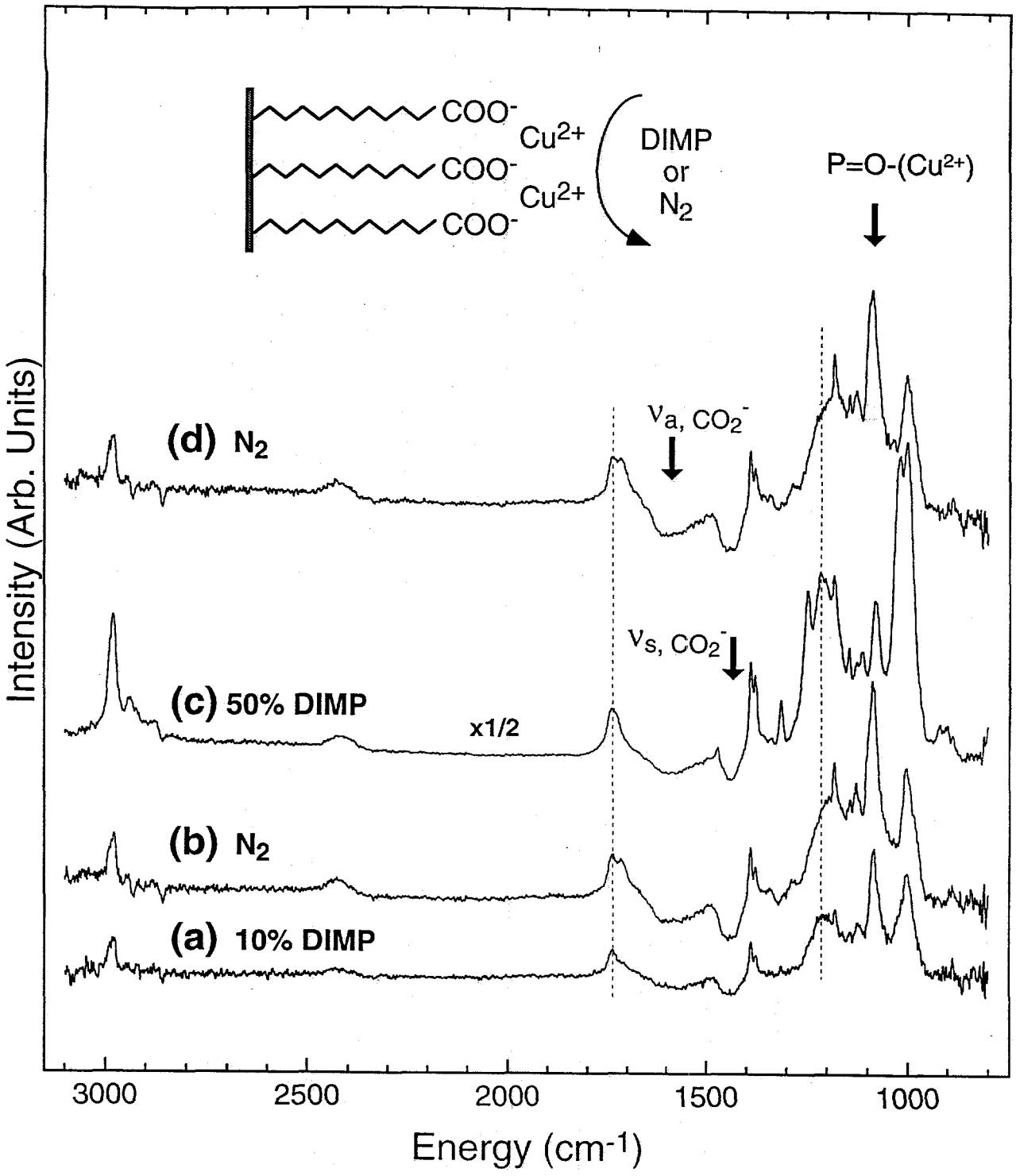

Figure 7/Crooks et al

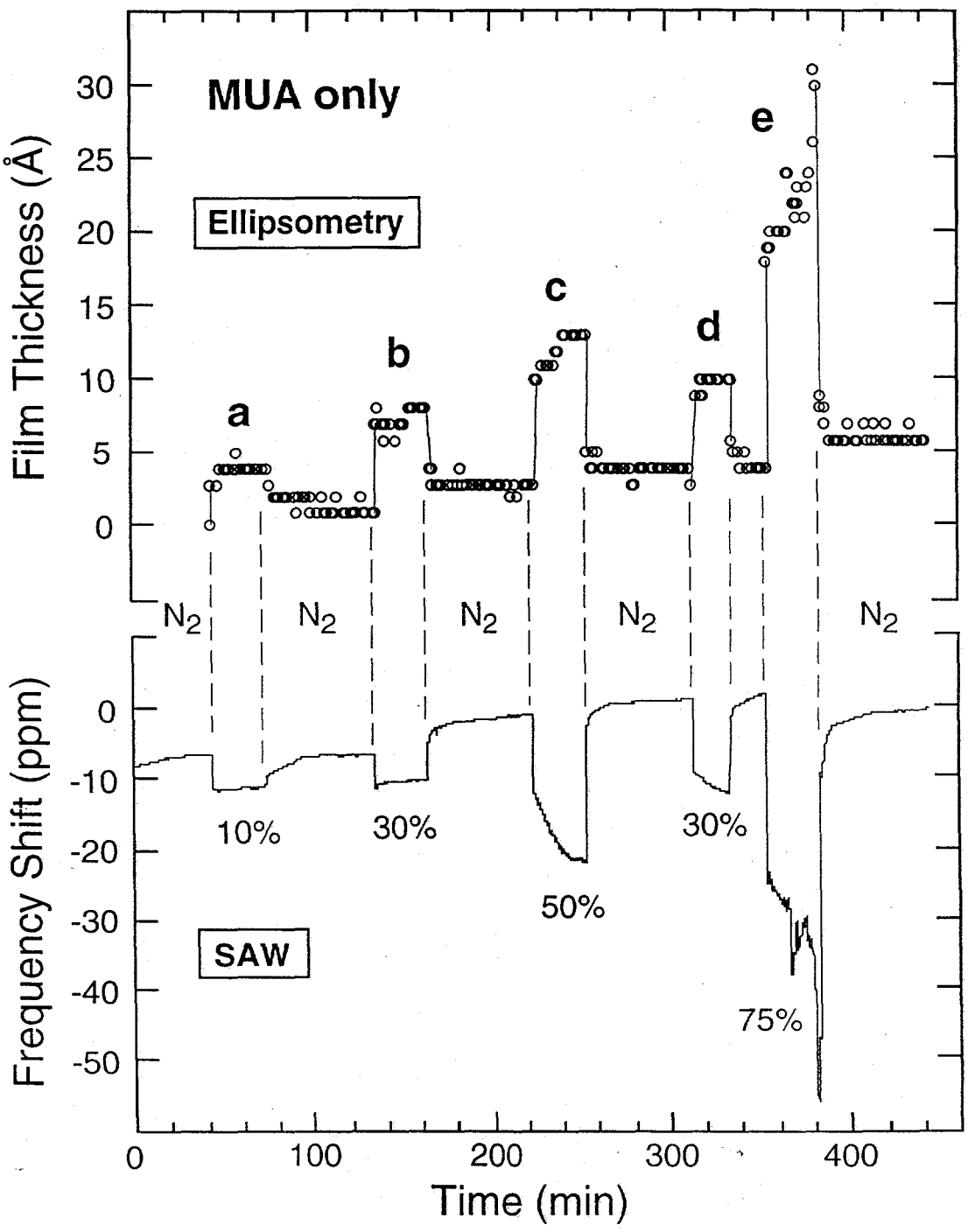

Figure 8/Crooks et al.

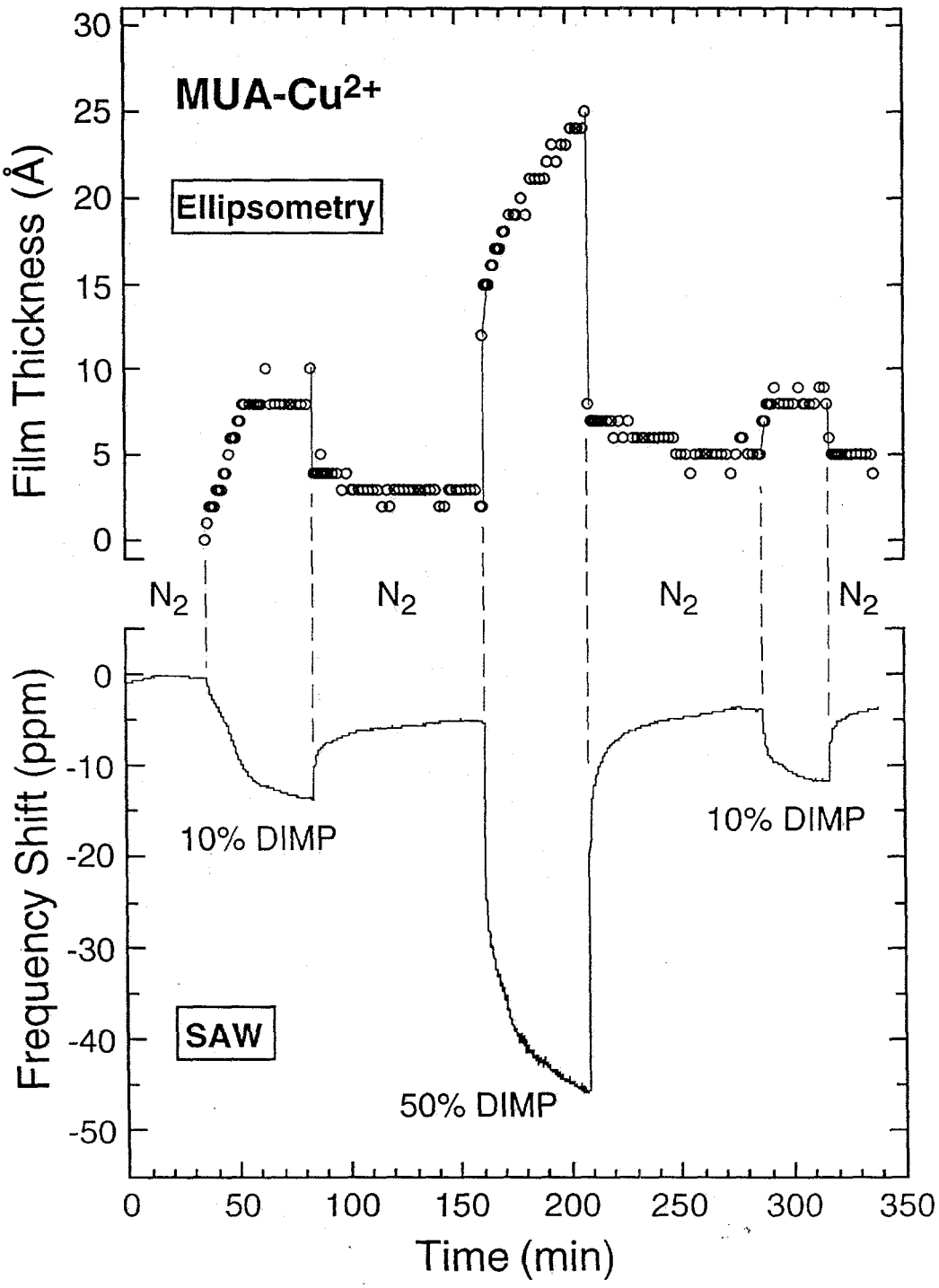

Figure 9/Crooks et al.

Supporting Material

Interaction of Self-Assembled Monolayers with an Organophosphonate: A Detailed study Using Surface Acoustic Wave Devices, IR Spectroscopy, and Ellipsometry

Richard M. Crooks*,[1], Huey C. Yang, and Laurel J. McEllistrem

Department of Chemistry

Texas A&M University

College Station, TX 77843-3255

Ross C. Thomas and Antonio J. Ricco*,[2]

Microsensor R&D 1425

Sandia National Laboratories

Albuquerque, NM 87185-1425

Figure Captions (Supporting Material)

Figure 1. PM-FTIR spectra of a MUA-Ag^{+} SAM during dosing with (a) 10%- and (c) 50%-of-saturation DIMP, and after purging with N_2 for 30 min (b and d). Dashed lines represent the hydrogen bonded phosphoryl band at 1207 cm^{-1} and non-hydrogen-bonded -COOH band at 1736 cm^{-1}. The asterisk marks the position of the metal-ion-complexed DIMP peak.

Figure 2. PM-FTIR spectra of a MUA-Cu^{2+} (from $CuCl_2$) SAM during dosing with (a) 10%- and (c) 50%-of-saturation DIMP, and after purging with N_2 for 30 min (b and d). Dashed lines represent the hydrogen bonded phosphoryl band at 1207 cm^{-1} and non-hydrogen-bonded -COOH band at 1737 cm^{-1}. The asterisk marks the position of the metal-ion-complexed DIMP peak.

Figure 3. PM-FTIR spectra of a MUA-Ni^{2+} SAM during dosing with (a) 10%- and (c) 50%-of-saturation DIMP, and after purging with N_2 for 30 min (b and d). Dashed lines represent the hydrogen bonded phosphoryl band at 1216 cm^{-1} and non-hydrogen-bonded -COOH band at 1740 cm^{-1}. The asterisk marks the position of the metal-ion-complexed DIMP peak.

Figure 4. PM-FTIR spectra of a MUA-Zn^{2+} SAM during dosing with (a) 10%- and (c) 50%-of-saturation DIMP, and after purging with N_2 for 30 min (b and d). Dashed lines represent the hydrogen bonded phosphoryl band at 1197 cm^{-1} and non-hydrogen-bonded -COOH band at 1740 cm^{-1}. The asterisk marks the position of the metal-ion-complexed DIMP peak.

Figure 5. PM-FTIR spectra of a MUA-Fe^{3+} SAM during dosing with (a) 10%- and (c) 50%-of-saturation DIMP, and after purging with N_2 for 30 min (b and d). Dashed lines represent the hydrogen bonded phosphoryl band at 1200 cm^{-1} and non-hydrogen-bonded -COOH band at 1741 cm^{-1}. The asterisk marks the position of the metal-ion-complexed DIMP peak.

Figure 6. PM-FTIR spectra of a MUA-La^{3+} SAM during dosing with (a) 10%- and (c) 50%-of-saturation DIMP, and after purging with N_2 for 30 min (b and d). Dashed lines represent the hydrogen bonded phosphoryl band at 1214 cm^{-1} and non-hydrogen-bonded -COOH band at 1740 cm^{-1}. The asterisk marks the position of the metal-ion-complexed DIMP peak.

Figure 7. PM-FTIR spectra of a MUA-Zr^{4+} SAM during dosing with (a) 10%- and (c) 50%-of-saturation DIMP, and after purging with N_2 for 30 min (b and d). Dashed lines represent the hydrogen bonded phosphoryl band at 1201 cm^{-1} and non-hydrogen-bonded -COOH band at 1740 cm^{-1}. The asterisk marks the position of the metal-ion-complexed DIMP peak.

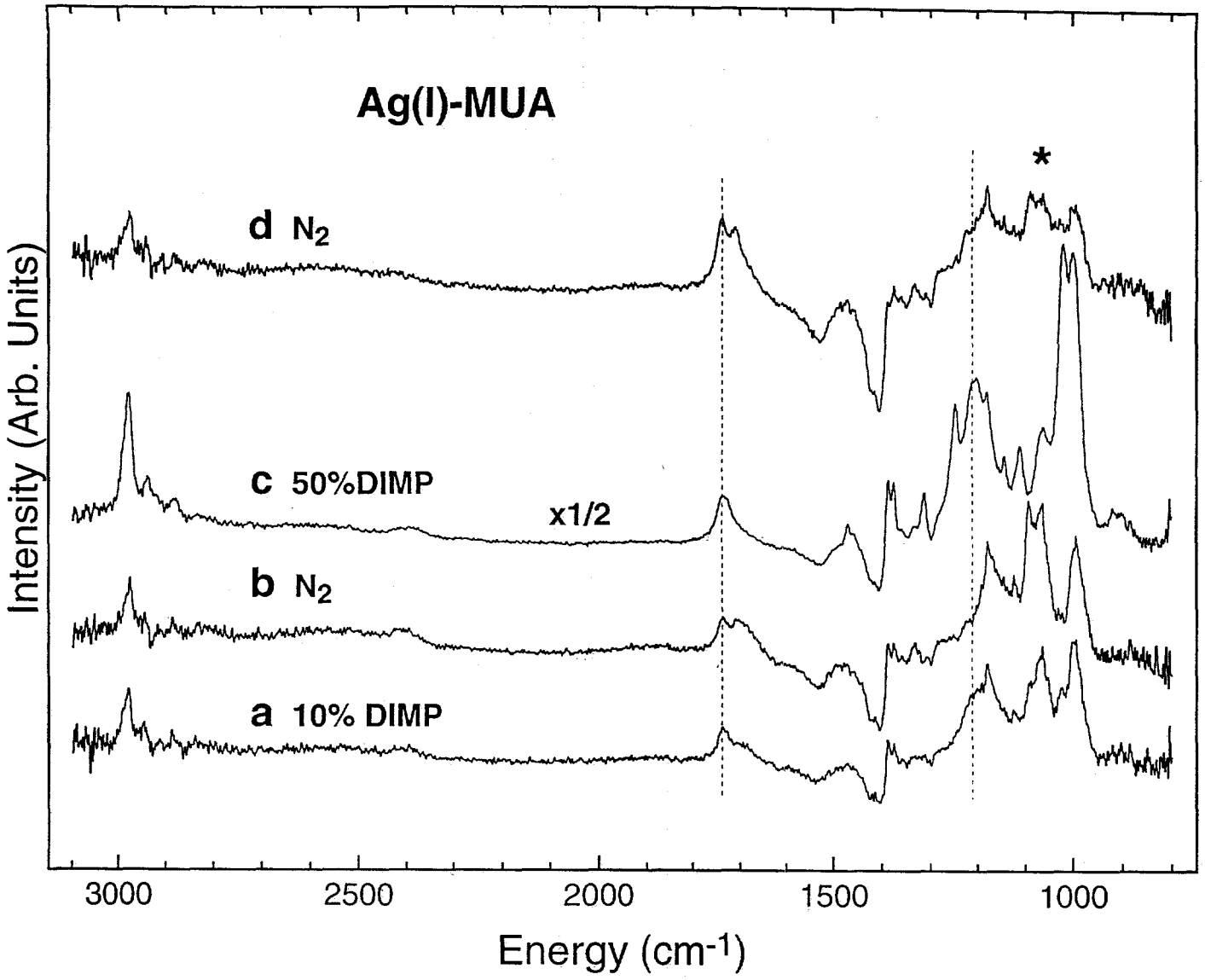

"Supporting Material.
Figure 1/Crooks etal."

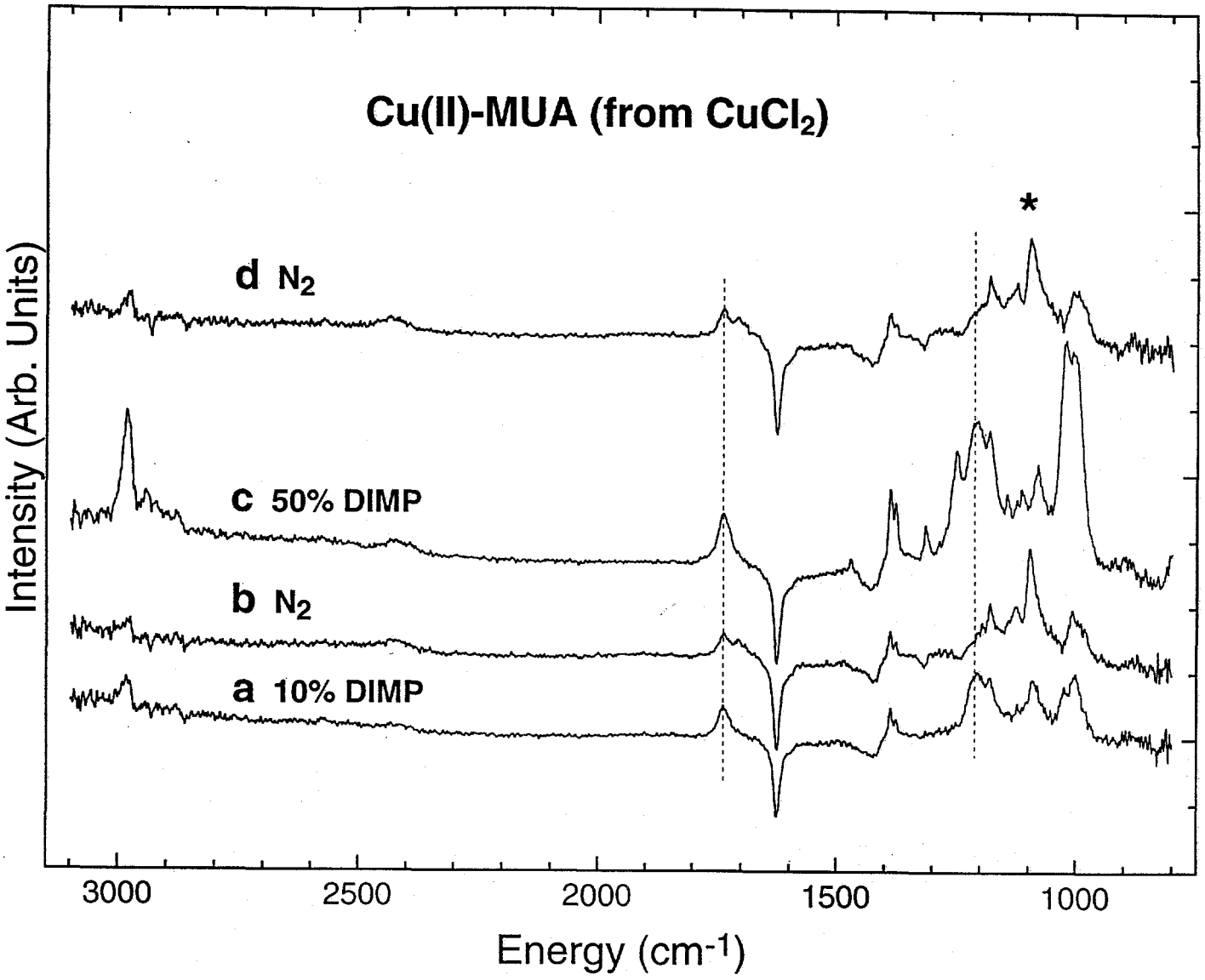

Supporting Material
Figure 2/Crooks et al.

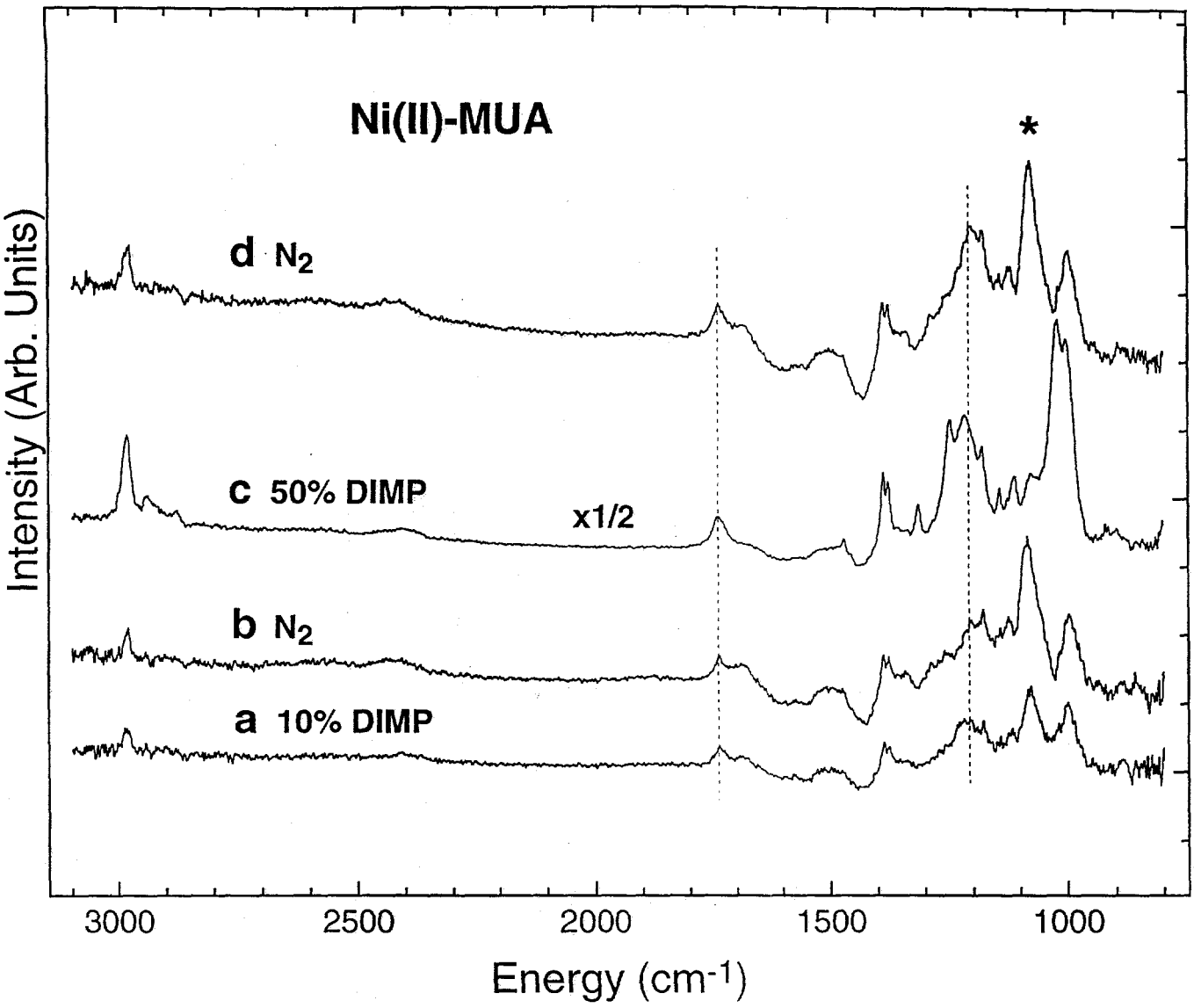

"Supporting Material.
Figure 3/Crooks etal".

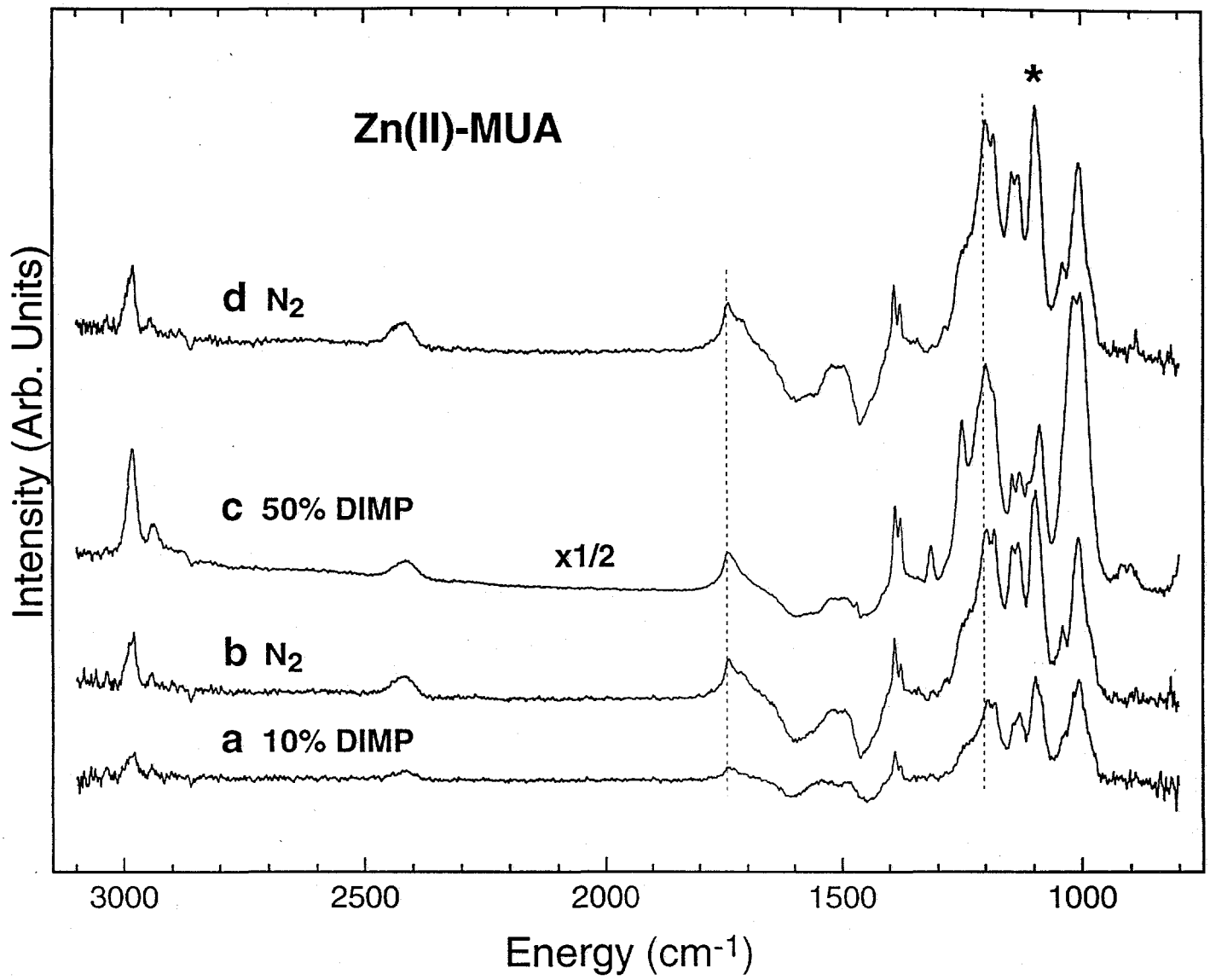

"Supporting Material.
Figure 4/Crooks etal."

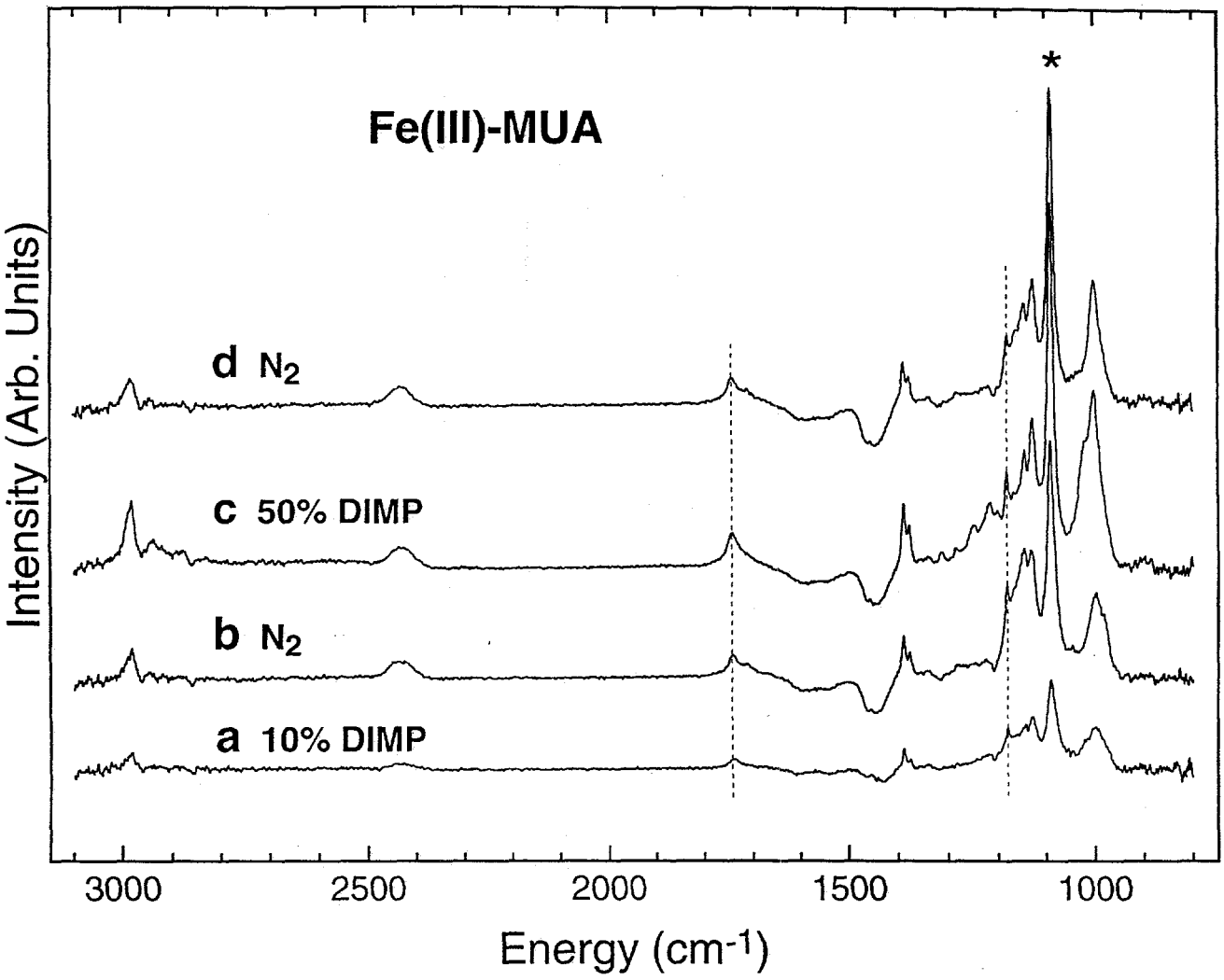

"Supporting Material.
Figure 5/Crooks etal."

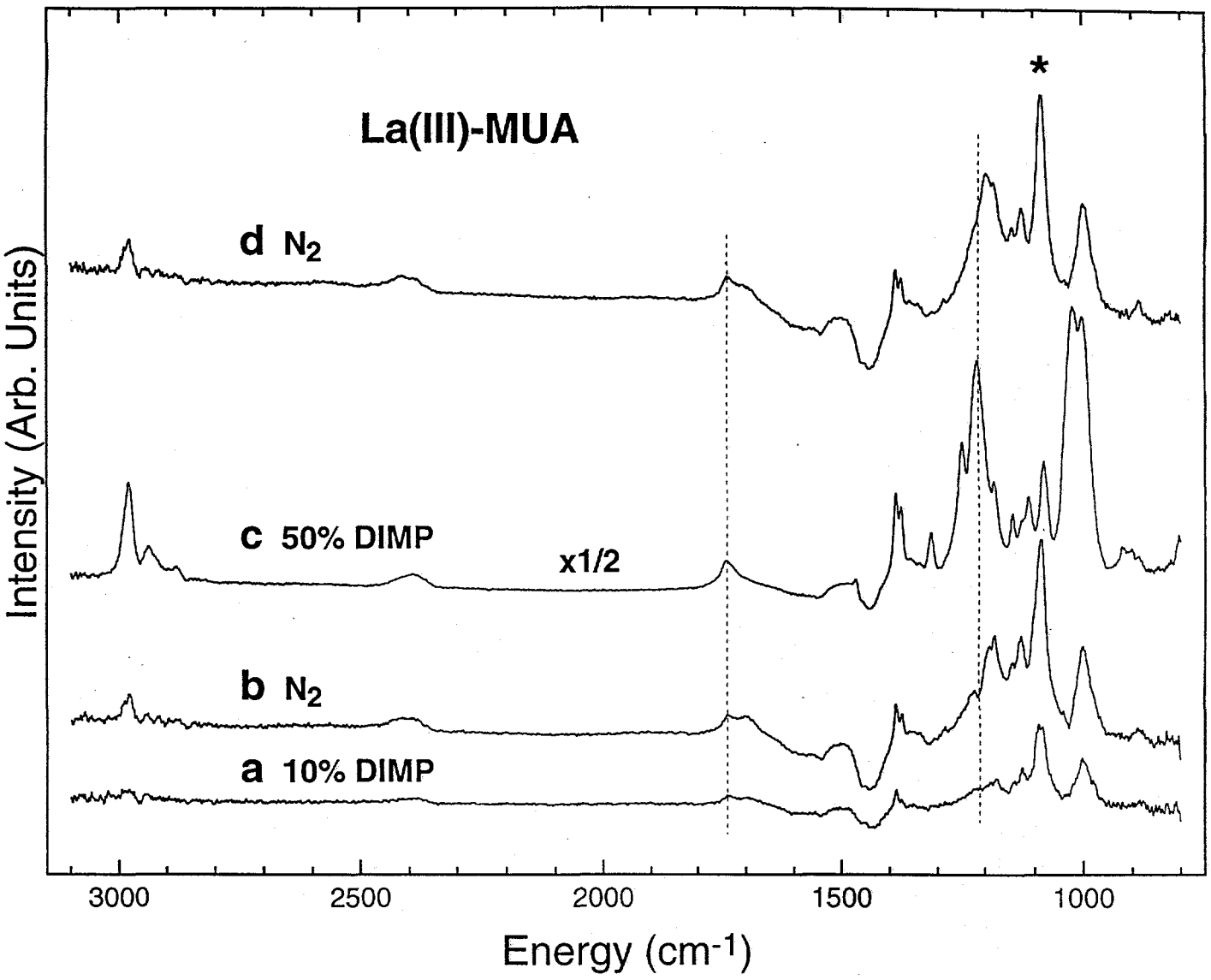

"Supporting Material.
Figure 6/Crooks etal."

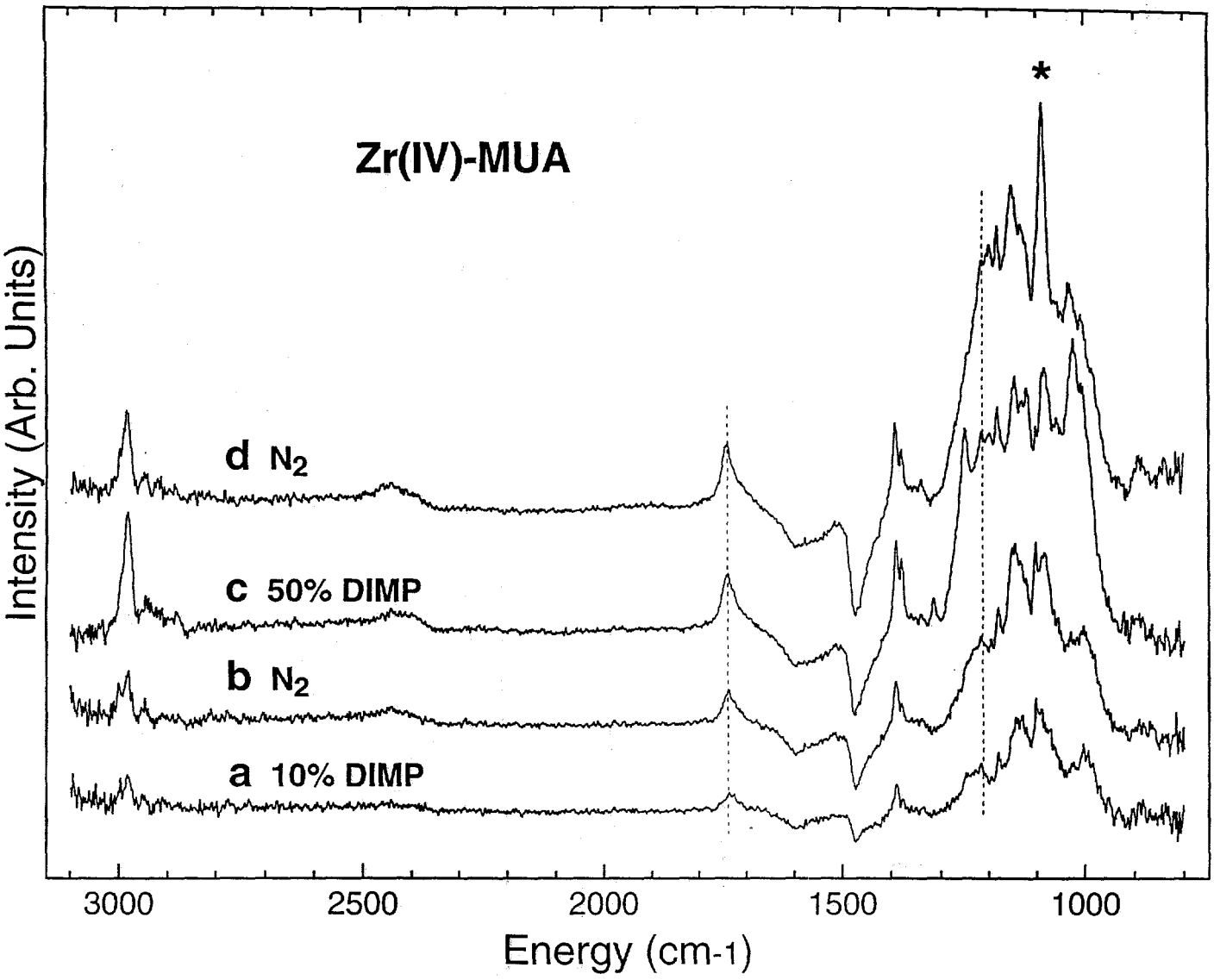

"Supporting Material.
Figure 7/Crooks etal."